Technical Report

TR-13-19

A review of the properties of pyrite and the implications for corrosion of the copper canister

Fraser King, Integrity Corrosion Consulting Limited

December 2013

Svensk Kärnbränslehantering AB
Swedish Nuclear Fuel
and Waste Management Co

Box 250, SE-101 24 Stockholm
Phone +46 8 459 84 00

ISSN 1404-0344
SKB TR-13-19
ID 1377791

A review of the properties of pyrite and the implications for corrosion of the copper canister

Fraser King, Integrity Corrosion Consulting Limited

December 2013

Keywords: Pyrite, Dissolution, Corrosion, Canister, Copper, Sulphide, Polysulphide, Bentonite.

Summary

A review of the properties of pyrite impurities in bentonite clay has been carried out based on information available in the literature. The main focus of the review is the extent to which pyrite dissolution during the long-term anaerobic period could support corrosion of the canister, most likely as the result of the release of dissolved sulphide or polysulphide species. In addition, the oxidative dissolution of pyrite has also been considered since processes occurring during the initial oxic period, and potentially continuing into the anaerobic phase, might affect the behaviour of pyrite during the anaerobic phase and its overall impact on canister corrosion.

Various aspects of the properties and behaviour of pyrite have been reviewed, including:

- the structure, composition, and electronic and thermodynamic properties of pyrite,
- surface characterisation and reactivity of pyrite,
- the relationship between pyrite and other iron sulphides,
- the characterisation of pyrite present in bentonite clays,
- attempts at mathematical modelling of the behaviour of pyrite in the repository,
- the aqueous speciation of sulphide and polysulphides,
- the solubility of pyrite and other iron sulphides,
- the dissolution behaviour of pyrite, including oxidative, reductive, and chemical (congruent) dissolution mechanisms,
- electrochemical studies of pyrite, and
- the expected behaviour of pyrite in the repository and the implications for the corrosion of the canister.

Based on the information available, it is considered unlikely that pyrite will be a significant source of sulphide or oxidants for corrosion of the canister. Instead, the predominant role of pyrite is likely to be the consumption of a fraction of the initially trapped atmospheric oxygen in the repository. The solubility of pyrite is so low that very little sulphide will be released during the long-term anaerobic phase even over repository timescales.

Contents

1 Introduction

Pyrite (FeS_{2p}) is the most common sulphide mineral in surface environments on the Earth and is found in sedimentary, igneous, and metamorphic geological formations, as well as in deep sea vents (Rickard and Luther 2007). (The p subscript is used here to distinguish pyrite from the dimorph marcasite FeS_{2m}). The oxidation of pyrite leads to the phenomenon of acid rock drainage which can have significant environmental impacts (Vaughan 2005). Pyrite is also the principal source of inorganic sulphur in coal (Zhao et al. 2005), the combustion of which results in air pollution and associated environmental effects.

Pyrite is an impurity mineral in bentonite and other clays proposed for use as sealing materials for the planned KBS-3 repository for the disposal of spent nuclear fuel in Sweden (Karnland 2010, Pusch 2001). The pyrite may have a number of effects on the evolution of the repository and the behaviour of the canister. First, oxidation of pyrite during the early warm, aerobic phase will consume a portion of the initially trapped atmospheric O_2 in the buffer and backfill materials (King et al. 2010, Puigdomenech et al. 2001). Second, during the long-term anaerobic phase, equilibria involving pyrite may control the redox potential E_h in the repository (Puigdomenech et al. 2001). Third, pyrite may be a source of sulphide ions HS^- for corrosion of the canister (SKB 2010a). For the SR-Site safety assessment, the extent of corrosion due to pyrite in the buffer is conservatively estimated based on a mass-balance approach, despite the belief that the availability of sulphide will be limited by the low solubility of pyrite. Corrosion due to the release of HS^- from pyrite in the backfill is treated using a mass-transport argument (SKB 2010a).

Figure 1-1 shows a schematic of different phases in the formation and alteration of pyrite in the context of the use of bentonite in the KBS-3 repository. Pyrite is formed either by precipitation from a high-temperature melt or by the precipitation of Fe(II) and HS^- and the subsequent ageing of a sequence of increasingly thermodynamically stable iron sulphides. The formation of bentonites also involves exposure to extreme temperatures and to aqueous environments, being the product of volcanic ash which is subsequently hydrothermally altered (Christidis and Huff 2009). Thus, either process is a feasible pathway for the formation of the pyrite found in bentonite deposits. Depending upon the environmental conditions to which the bentonite deposit is exposed, alteration of the pyrite is possible over geological timescales prior to exploitation of the deposit. Mining and processing of the raw bentonite may also expose the pyrite impurities to further (oxidation) alteration. Once emplaced in the repository, the pyrite will be exposed to a warm, aerobic phase and may undergo further alteration. Finally, once anaerobic conditions have become established in the repository, pyrite may dissolve and release sulphide ions. The focus of the current review is the potential for pyrite to act as a source of sulphide for canister corrosion during this latter long-term anaerobic phase, although it is important to understand that the original pyrite phase may have been extensively altered during the intervening periods.

Pyrite is an Fe(II) polysulphide with a cubic crystal structure and exhibits semiconducting properties (Rickard and Luther 2007). Thus, the dissolution behaviour of pyrite can be discussed in electrochemical terms, with both oxidative and reductive dissolution mechanisms possible (Figure 1-2). Under oxidising conditions in the presence of O_2 or Fe(III), pyrite will dissolve oxidatively with the formation of Fe(II) and SO_4^{2-} (note, it is the polysulphide species that is oxidised rather than the metal species). Under reducing conditions, FeS_{2p} dissolves with the release of HS^- (i.e., the polysulphide species S_2^{2-} with a nominal average oxidation state of –I is reduced to a sulphide with oxidation state –II). Under natural conditions, the reduction of FeS_{2p} must be accompanied by the oxidation of a suitable reducing species. At intermediate E_h values, pyrite may dissolve chemically with the release of Fe(II) and S_2^{2-}, with the latter species undergoing disproportionation in the aqueous phase. In terms of the various stages illustrated in Figure 1-2, the focus of the current report is on the chemical and reductive dissolution processes.

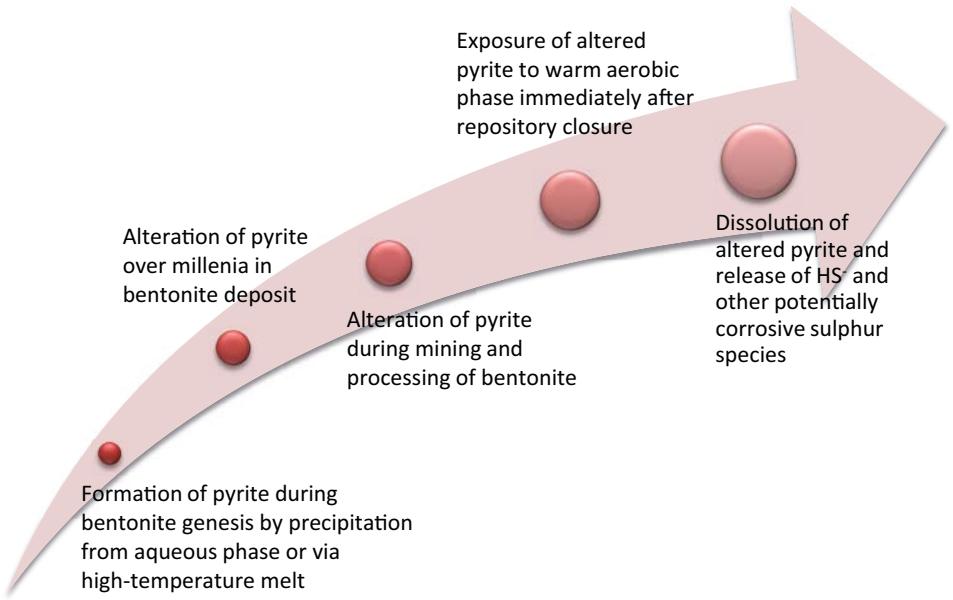

Figure 1-1. *Lifecycle of pyrite from formation in bentonites to alteration in the repository.*

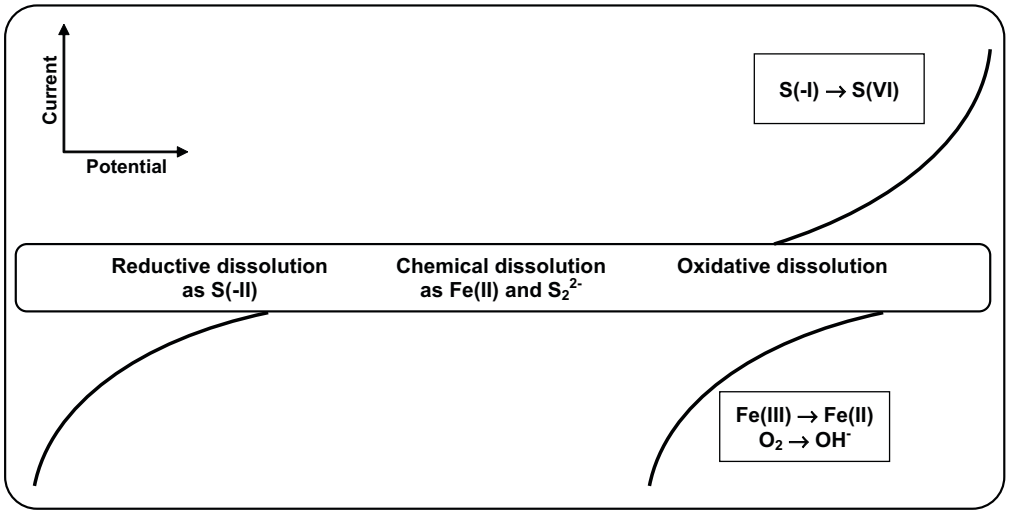

Figure 1-2. *Schematic of the electrochemical behaviour of pyrite.*

Various aspects of the dissolution behaviour of pyrite are reviewed here. First, the properties of pyrite are described, including the crystal structure, electronic, and thermodynamic properties. The relationship of pyrite to other iron sulphides is also discussed, since transformation of pyrite to other more-soluble phases could represent a route by which higher concentrations of dissolved sulphide could occur. Next, the nature and extent of pyrite in bentonite clay are considered, although the available information is limited because of the difficulties associated with characterising minor phases. In the next two sections, the aqueous chemistry of dissolved sulphur species and the solubility of solid iron sulphides are discussed. The speciation of aqueous sulphur species is relevant as pyrite may dissolve with the release of sulphate, polysulphide, or sulphide, depending upon the redox potential. The solubilities of mackinawite and greigite as well as that of pyrite are considered here. The dissolution behaviour of pyrite is discussed in the next section, with a brief description of the oxidative dissolution mechanism, a more-detailed review of the available information on reductive dissolution, and a summary of the chemical dissolution behaviour. In addition, the electrochemical behaviour of FeS_{2p} is also discussed. Finally, implications of the foregoing information for the dissolution behaviour of pyrite in the repository under oxic and anaerobic conditions and the implications for corrosion of the canister are summarised.

2 Properties of pyrite and associated iron sulphides

2.1 Pyrite

2.1.1 Structure

Pyrite is an Fe(II) polysulphide with the nominal composition FeS_{2p}. Pyrite has a cubic NaCl-type structure with Fe(II) at the cube corners and face centres and S_2^{2-} at the cube centre and at the mid-points on the cube edges. Figure 2-1 shows the crystal structure of pyrite, with the polysulphide ions orientated as shown (Rickard and Luther 2007). Because of the arrangement of the polysulphide, pyrite exhibits a lower degree of symmetry than NaCl and consequent chirality, which results in differences in reactivity of different crystal planes.

2.1.2 Composition

Although close to stoichiometric, naturally occurring pyrite exhibits a wide range of minor and trace elements (Abraitis et al. 2004). Trace elements, defined here as species with a maximum concentration of 0.1 wt.% (1,000 wppm) include Te, Sn, Se, Ru, Pt, Pd, Cd, and Ag. Minor elements found with maximum concentrations of 1 wt.% (10,000 wppm) include Zn, Tl, Sb, Pb, Ni, Hg, and Au. The impurity elements found at highest concentration in natural pyrites (in the range 1–10 wt%) are Mo, Cu, Co, and As. The latter two impurity elements are interesting because of their impact on the semi-conducting natural of pyrite, with As also of particular interest because of the environmental issues associated with acid rock drainage. These minor and trace elements can be present as either substitutions in the pyrite lattice or as inclusions.

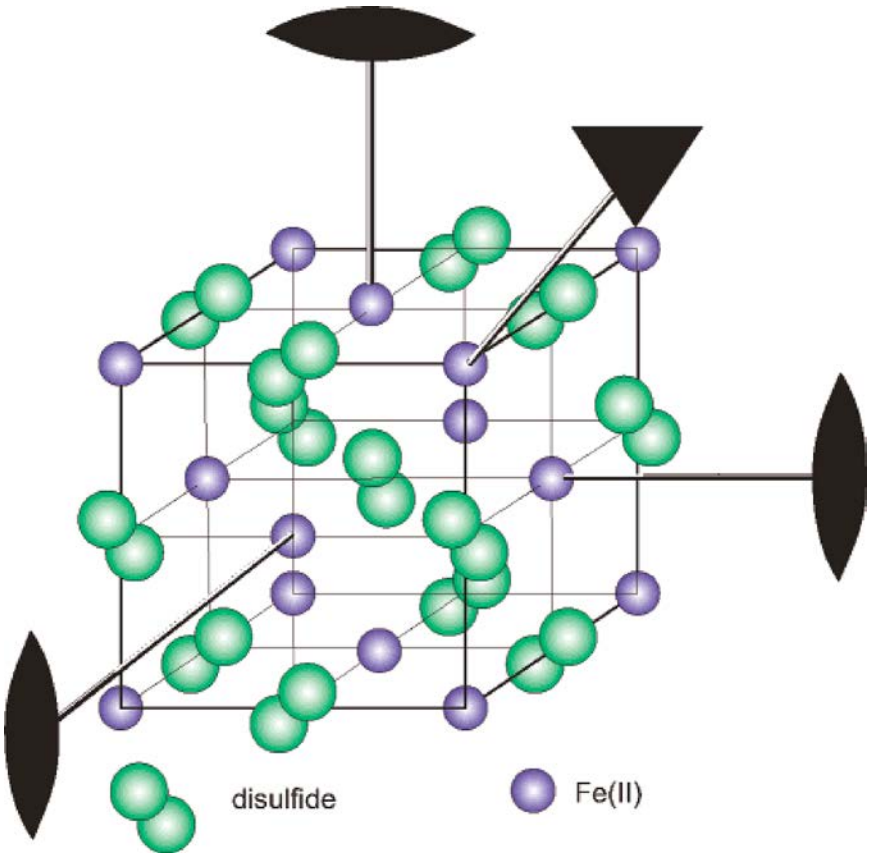

Figure 2-1. *Crystal structure of pyrite FeS_{2p} (Rickard and Luther 2007). The major axes of symmetry are also shown in the figure.*

2.1.3 Semi-conductivity

Pyrite exhibits both n-type and p-type semi-conductivity and has a band gap of ~0.9 eV (Vaughan 2005). Various conduction and valence band structures have been proposed (Murphy and Strongin 2009). The nature of the impurities and the manner in which the pyrite was formed tends to determine the type of semi-conductivity and the electrical resistivity (Savage et al. 2008). Pyrite formed in sedimentary deposits at lower temperatures is primarily a p-type semi-conductor in the absence of Cu, as are As-containing pyrites or pyrites with a S:Fe ratio > 2. Pyrite formed at higher temperatures tends to be n-type (in the absence of As), as are pyrites containing Co as an impurity and pyrites with S:Fe < 2. Although the resistivity of pyrites varies over a wide range, pyrites exhibiting p–type semi-conductivity tend to be more resistive (reported resistivities of 0.5–35 Ω·cm) than n-type pyrites (resistivities 0–0.64 Ω·cm) (Abraitis et al. 2004, Savage et al. 2008).

2.1.4 Thermodynamic properties

Various publications list thermodynamic properties for FeS_{2p} although many of them are references to other studies, with apparently few original sources. Table 2-1 lists a number of the reported standard free energy of formation (ΔG_f^0) values along with a description of their source. The majority of values that have been reported are between –159.5 kJ/mol and –160.23 kJ/mol, although only two original experimental sources have been found (Grønvold and Westrum 1976, Toulmin and Barton 1964). The value of –166.9 kJ/mol listed in the US National Bureau of Standards compilation (Wagman et al. 1982) may be in error due to an error in the ΔG_f^0 value for Fe^{2+} (Rickard and Luther 2007). For the current purposes, the ΔG_f^0 value of –160.229 kJ/mol from Robie et al. (1978) is used for the solubility calculations in Section 5.2.

2.1.5 Surface characterisation

Characterisation of the nature of the pyrite surface is important for understanding a range of important industrial and natural processes involving pyrite, including the oxidation behaviour, flotation of pyrite during mineral and coal processing, and the interaction with metal ion contaminants. Studies have been performed with naturally weathered samples, crushed and ground pyrite, as well as freshly fractured ("pristine") pyrite surfaces.

Pyrite does not exhibit the preferential cleavage along the [001] crystal plane typical of minerals with a rock salt structure, but instead fractures conchoidally, i.e., along a curved fracture plane (Nesbitt et al. 1998). Pyrite has both Fe-S and S-S bonds, with the weaker S-S cleaving preferentially. The resulting exposed S atoms with a formal oxidation state of –I relax via an electron transfer from Fe(II), resulting in surface S(–II) and Fe(III) species, rather than by electron transfer between S atoms resulting in S(0) and S(–II) species (Nesbitt et al. 1998). The surface S(–II) represents an impurity defect site, in addition to the structural defects on the surface (kinks, Fe vacancies, steps), all of which impact the reactivity of the pristine cleaved surface.

Of more interest here is the nature of the naturally weathered pyrite surface. A range of iron surface species have been proposed for the weathered (oxidised) surface, including: ferrous carbonate (siderite) or sulphate, with small amounts of goethite (α-FeOOH) (Descostes et al. 2001); α-FeOOH, hematite α-Fe_2O_3, or magnetite Fe_3O_4 (Cai et al. 2009); ferric sulphate $Fe_2(SO_4)_3$, ferric hydroxide $Fe(OH)_3$, and FeO (de Donato et al. 1993); and hydrated Fe(III) (Joeckel et al. 2005). The range of proposed surface sulphur species is, if anything, more diverse, and includes: polysulphide S_n^{2-}, sulphur-oxyanions, such as thiosulphate $S_2O_3^{2-}$ (Descostes et al. 2001); molecular sulphur S_8 (Toniazzo et al. 1999); sulphite SO_3^{2-}, sulphate SO_4^{2-}, $S_2O_3^{2-}$, and S_8 (Cai et al. 2009), and polysulphide S_6^{2-} and S_8 (de Donato et al. 1993). In addition, a range of other mineral phases has also been reported, including: gypsum $CaSO_4 \cdot 2H_2O$ and alumino-sulphate minerals (Joeckel et al. 2005); and a range of Al and Si alteration products, such as alunite $KAl_3(SO_4)_2(OH)_6$, jarosite $KFe_3(SO_4)_2(OH)_6$, and gibbsite $Al(OH)_3$ formed by the precipitation of the constituents of aluminosilicate minerals dissolved in the low pH conditions associated with the oxidative dissolution of pyrite (Langmuir 1997).

It is apparent, therefore, that a range of species can be expected in the crust of alteration products on weathered pyrite surfaces. Most importantly for the current discussion is that these alteration products can include polysulphide species, which could then dissolve and dissociate into sulphide ions HS^-, and Fe(III) species, which could promote oxidative dissolution of pyrite once anaerobic conditions have become established in the repository.

Table 2-1. Summary of reported free energy of formation values for pyrite.

ΔG_f^0 (kJ/mol)	Uncertainty (kJ/mol)	Reference	Source
–166.9		Wagman et al. 1982	Not given
–160.1*		Singh and Pourbaix 1997	Reference to another CEBELCOR report
–160.229	1.715	Robie et al. 1978	Reference to Toulmin and Barton 1964
–160.1	1.7	Robie and Hemingway 1995	References to Toulmin and Barton 1964 and Chase 1985
–160.060		Chase 1998	Not given
–160.1		Kaye & Laby 2005	Not given
–166.9		Kaye and Laby 1986	Not given
–162.2*	2.1	Grønvold and Westrum 1976	Based on original heat capacity measurements by authors
–159.5*		Toulmin and Barton 1964	Based on original experimental study by the authors
–160.23		Benning et al. 2000	Reference to Robie et al. 1978
–159.5		Rickard and Luther 2007	Inferred value from $K^*_{1sp,pyrite}$ value of $10^{-14.2}$
–160.1		Hummel et al. 2002	Reference to Robie and Hemingway 1995
–160.2		Langmuir 1997	Reference to Robie et al. 1978

* Converted from cal/mol based on 1 cal = 4.184 J.

2.1.6 Surface reactivity – gas phase studies

Different crystal planes exhibit different reactivity. By necessity, the reactivity of different crystal planes has been studied under well-controlled environmental conditions, often under vapour or gas phase conditions under partial vacuum where the effects of different surfaces are more apparent (Murphy and Strongin 2009). The most commonly studied surface is the [100] plane. In the gas phase, H_2O adsorbs via an Fe-O interaction but, most importantly, the water does not dissociate and can be desorbed again as H_2O. Similarly, the exposure of a [100] pyrite surface to H_2S results in adsorption of the gaseous species (and subsequent desorption) without any indication of reaction with the pyrite surface (at temperatures below 500 K). On the assumption that these observations can be extrapolated to aqueous conditions, these results would imply that the presence of H_2O and/or HS^- under anaerobic conditions in the repository will not cause any alteration of the (pristine) pyrite surface.

In contrast to the behaviour of H_2O and H_2S, O_2 and especially O_2/H_2O gas mixtures (Elsetinow et al. 2000, Guevremont et al. 1998a, b) cause oxidation of pyrite (Murphy and Strongin 2009). Oxygen alone results in the formation of Fe-O bonds and the oxidation of S^{2-}, indicating a degree of electron transfer. In the presence of O_2, H_2O does dissociatively adsorb (unlike in the absence of O_2), with the oxygen from the H_2O molecule becoming incorporated into the SO_4^{2-} formed when pyrite is oxidised by O_2 or Fe(III).

In the presence of (humid) air under atmospheric conditions, pyrite surfaces oxidise (Murphy and Strongin 2009). The [111] plane is more reactive than the [100] plane, possibly because of more Fe atoms on the [111] plane or because of enhanced dissociative adsorption of water on the [111] plane. Surface Fe species play a key role in the oxidation of pyrite by O_2, with electron transfer between adsorbed Fe(II) and Fe(III) species promoting the cathodic reduction of O_2, the first electron transfer to which is considered to be the rate-determining step. Blocking or chelating Fe(III) surface sites suppresses pyrite oxidation. Surface sulphur species are also oxidised, with surface S oxidised to SO_4^{2-} and sub-surface S oxidised to SO_3^{2-} (Murphy and Strongin 2009). A notable feature of these surface studies is that the oxidation is heterogeneous across the surface with patches of Fe(II)/Fe(III) species.

Because of the absence of a preferred cleavage plane for pyrite, crushed or ground pyrite samples exhibit a range of reactivity due to the presence of different crystal planes of different reactivity. The most common surface plane in crushed samples is the [100] plane, with additional amounts of [021], [111], and [110] planes (Murphy and Strongin 2009).

2.1.7 Interaction with metal ions

The interaction of pyrite with metal cations has been extensively studied, because of the importance of the activation of pyrite during flotation, the co-precipitation and recovery of precious metals such as gold, and the sequestration of metal contaminants (Murphy and Strongin 2009). These studies

have included the study of the adsorption of Cu(II) by pyrite, primarily due to the effect of Cu in enhancing pyrite separation by flotation (von Oertzen et al. 2007), but of interest here because of the presence of Cu(II) in the bentonite in the transitional period between aerobic and anaerobic phases in the evolution of the repository environment.

There is near-unanimous agreement among different authors that the adsorption of Cu(II) is accompanied by the reduction of the adsorbate to Cu(I) and the oxidation of the adsorbent (FeS_{2p}). Where there is no agreement is on the nature of the oxidised species. Using X-ray photoelectron spectroscopy (XPS) with and without the use of synchrotron radiation, von Oertzen et al. (2007) showed that Cu(I) was bound to both monosulphide (Fe-S^{2-}) and polysulphide (Fe-S_2^{2-}) sites on the pyrite surface. By analogy with other studies, the authors proposed that the overall adsorption reaction involved the oxidation of pyrite to sulphate, according to:

$$FeS_{2p} + 3xCu^{2+} + 4xH_2O \rightarrow Cu_{3x}FeS_{2-x} + xSO_4^{2-} + 8xH^+ \quad (2\text{-}1)$$

Laajalehto et al. (1999) found that the Cu:Fe ratio on the surface increased with decreasing E_h in acid solution (but not at pH 9) and suggested the formation of a chalcopyrite $CuFeS_2$-type surface layer. This would infer that the reduction of Cu(II) to Cu(I) is accompanied by the oxidation of Fe(II) to Fe(III), reflecting the oxidation states of these species in chalcopyrite. Weisener and Gerson (2000) proposed the formation of an oxidised polysulphide which they denoted $S_2^{2-}{}_{ox}$, but it is not clear what such a species is and whether sulphide is released to solution as a consequence. Using a combination of XPS, X-ray absorption near-edge structure (XANES), and extended X-ray absorption fine structure (EXAFS), Naveau et al. (2006) were unable to find any oxidation products on the surface of pyrite on which cupric ions had been reduced to Cu(I) and concluded that the reductive adsorption process was accompanied by the oxidation of S_2^{2-}, the products of which had gone into solution.

2.2 Formation of pyrite and its relationship to other iron sulphides

Pyrite is just one of a large number of iron sulphides found in natural systems. Table 2-2 lists some of the more common minerals found along with some of their selected properties (Rickard and Luther 2007). The inter-relationship between these sulphides is important as any process that may lead to the conversion of pyrite to a less thermodynamically stable iron sulphide could lead to an increase in the concentration of dissolved HS^-.

Figure 2-2 shows the inter-relationship between the various iron sulphides, with known processes indicated by the solid lines and inferred processes indicated by the dashed lines. This figure should not be interpreted as indicating that the conversion from one phase to another occurs via a solid-state process. Although this is possible in some cases, conversion from one sulphide to another is also possible by the dissolution and re-precipitation of Fe(II), and/or dissolved sulphide and polysulphide species. In general, the progression from left to right in the figure corresponds to the formation of increasingly thermodynamically stable solids. There is no indication in the literature that any of these transformations is reversible, i.e., once the more stable iron sulphide is formed it is not subsequently converted to a less-stable solid (Butler and Rickard 2000).

Table 2-2. Summary of solid iron sulphides and their properties.

Mineral	Composition	Structure	Properties
Mackinawite	FeS_m	Tetragonal	Metastable, principal species formed by precipitation of Fe(II) in aqueous solution
Cubic FeS	FeS_c		Unstable, formed prior to FeS_m
Troilite	FeS_t		Stoichiometric end-member of the pyrrhotite group
Pyrrhotite	$Fe_{1-x}S$	Various	Stable, non-stochiometric iron sulphide with $x < 0.2$
Greigite	Fe_3S_{4g}	Inverse spinel	Metastable mixed Fe(II)/Fe(III) inverse thiospinel
Pyrite	FeS_{2p}	Cubic	Stable Fe(II) disulphide
Marcasite	FeS_{2m}		Metastable Fe(II) disulphide

In aqueous solution, mackinawite FeS_m is the predominantly observed solid phase when Fe or Fe(II) first reacts with HS^- or H_2S, particularly in environments with excess Fe(II). The kinetics of FeS_m precipitation are fast, with the mackinawite typically formed as nanoparticulate material (Rickard and Luther 2007). So-called "amorphous FeS" is sometimes reported and can be viewed as a precursor of FeS_m which forms from the ageing of the amorphous material. Mackinawite is metastable with respect to pyrite but is not a necessary precursor to pyrite formation. Because of a common cubic close packed sulphur lattice, however, mackinawite can convert to greigite Fe_3S_{4g} via a solid state process involving rearrangement of Fe atoms. Greigite exhibits an inverse spinel structure, with Fe(II) in tetrahedral sites and Fe(II) and Fe(III) sharing octahedral lattice positions. Chemically, the formation of Fe_3S_{4g} from FeS_m involves only the oxidation of Fe(II) to Fe(III), since both are sulphides. In contrast, since FeS_{2p} is an Fe(II) polysulphide, the formation of pyrite from mackinawite would formally involve the oxidation of S(–II) to S_2^{2-} but no change in oxidation state of the Fe. The alternative route for the formation of FeS_{2p} is via the sulphidation of pyrrhotite (or troilite). (Figure 2-2).

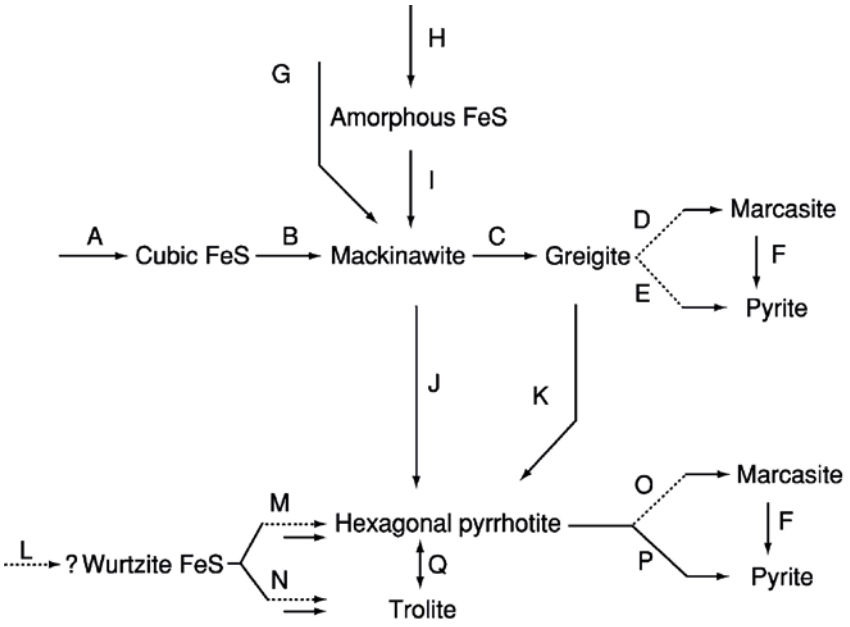

A	formation from Fe^{2+} or Fe and HS^- or H_2S at a pH of 4–5 (T < 523 K)
B	ageing of cubic FeS to FeS_m
C	solid-state conversion of FeS_m to Fe_3S_{4g}
D	inferred transformation of greigite to marcasite
E	inferred sulphidation of greigite at pH > 5 (T < 523 K)
F	solid state transformation
G	sulphidation of Fe by H_2S at a pH of 3–10 (T < 523 K)
H	precipitation of dissolved Fe^{2+} and HS^-
I	ageing of amorphous precipitate
J	solid state transformation, kinetics not established
K	transformation of greigite to pyrrhotite
L	precipitation of Fe^{2+} by HS^- at pH 4–6 (wide range of temperatures to above 573 K)
M,N	reaction of Fe^{2+} and HS^- or H_2S at a pH 4–5 (or speculative transformation of proposed wurtzite-FeS structure) to form either (M) hexagonal pyrrhotite (T > 413 K) or (N) troilite (T < 413 K)
O	pyrrhotite transformation to marcasite
P	pyrite formed by sulphidation of pyrrhotite (this reaction is rapid above 573 K)
Q	troilite–hexagonal pyrrhotite reversible phase transition

Figure 2-2. *Inter-relationship between various iron sulphide solid phases (Vaughan 2005). The solid and dashed lines indicate known and speculative processes, respectively.*

The discussion above focuses on the formation of pyrite via dissolution-precipitation processes in the aqueous phase, which is the most likely pathway for pyrite formed in sedimentary deposits (Schoonen 2004). However, nucleation of pyrite from solution requires a considerable degree of supersaturation of the solution (Rickard and Luther 2007). An alternative route is via the cooling of high-temperature molten systems (Vaughan 2005). Since bentonite is formed from the weathering of volcanic ash, the pyrite may have formed as a high-temperature melt and then been dispersed with the ash during an igneous event.

The relative thermodynamic stabilities of the different iron sulphides can be represented on E-pH diagrams (Rickard and Luther 2007, Singh and Pourbaix 1997, Vaughan 2005). Figure 2-3 shows the potential-pH stability diagram for the Fe-S-H_2O system at 25°C, illustrating the relative thermodynamic stabilities of the different iron sulphides and oxides. At high dissolved sulphur activity ($a_S^{tot} = 0.1$, Figure 2-3A), pyrite is predicted to be stable over a wide range of pH under relatively reducing conditions. The extent of the pyrite stability field diminishes with decreasing S activity ($a_S^{tot} = 10^{-6}$, Figure 2-3B), with Fe_3O_4 predicted to be more stable at pH > 9. More interestingly, under moderately alkaline conditions and at the H_2O/H_2 equilibrium potential and slightly higher, pyrrhotite FeS is more stable than FeS_{2p}. This would imply that, in an environment that becomes increasingly anaerobic, pyrite could be reduced to pyrrhotite (involving the reduction of S_2^{2-} to S^{2-}), although there are no reports of such a process occurring in nature and the reaction could be kinetically hindered (see Section 6.2).

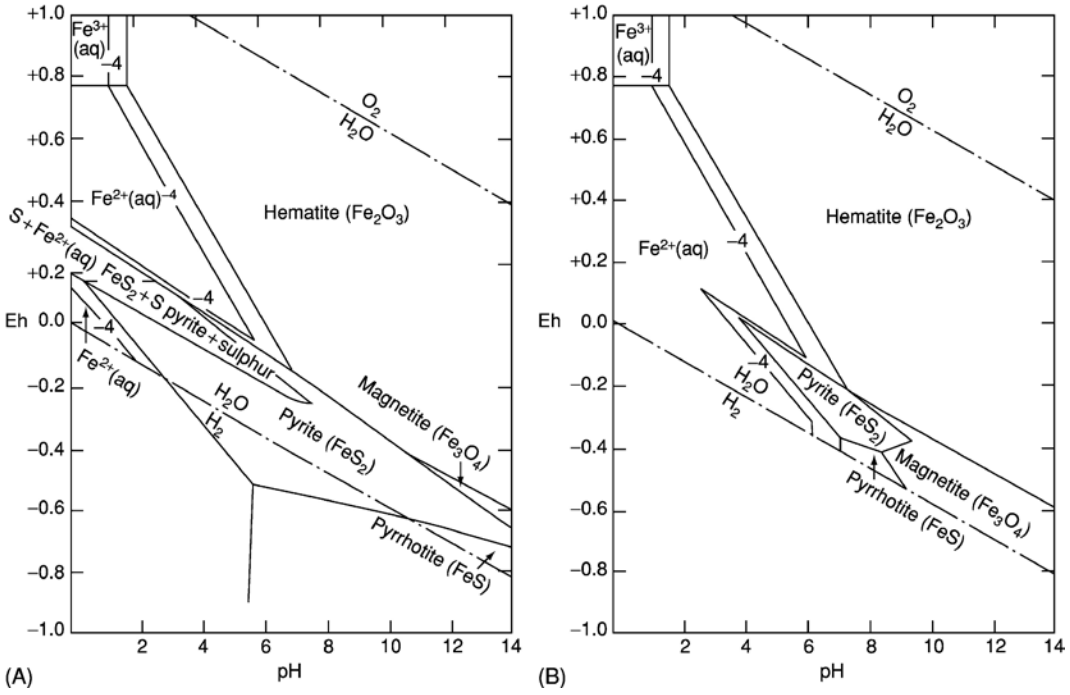

Figure 2-3. *Potential-pH diagrams for the Fe-S-H_2O system at 25°C at 1 atm total pressure and for total dissolved sulphur activities of (A) 0.1 and (B) 10^{-6} (Vaughan 2005).*

3 Pyrite in bentonite

3.1 Background

Pyrite is present as one of a number of accessory minerals in bentonite, a list that includes quartz, feldspars, gypsum, and various iron oxides/hydroxides (Karnland 2010). Although only present in minor amounts, pyrite influences the evolution of the repository environment in a number of ways:

- Consumption of the initially trapped O_2 leading to the onset of anoxic conditions (Grandia et al. 2006, Lazo et al. 2003, Puigdomenech et al. 2000, 2001, Sidborn and Neretnieks 2003, Wersin et al. 1994).
- Acting as a potential source of sulphide for corrosion of the canister (King et al. 2011a, b, SKB 2010a).
- Controlling the redox conditions during the long-term anoxic phase (Arcos et al. 2008, Pusch 2003).
- Immobilising radionuclides released from the spent fuel after failure of the canister (Bruggeman et al. 2007, Delécaut 2004, Descostes et al. 2010, Scott et al. 2007).

Of these different processes, the one of current interest is the release of HS^- ions and the subsequent corrosion of the canisters. In order that the buffer material not significantly impair the barrier function of the canister, one of the design premises for the buffer is that (SKB 2010b):

> *The sulphide content should not exceed 0.5 wt-% of the total mass, corresponding to approximately 1% of pyrite.*
>
> *The total sulphur content (including the sulphide) should not exceed 1 wt-%.*

Along with a limit on the organic carbon content of the buffer, this design premise has been established to minimise the extent of canister corrosion based on the assumption that pyrite dissolution under anaerobic conditions is a source of sulphide ions.

In this Chapter, the available information on the occurrence and nature of pyrite in bentonite and sedimentary host rocks is reviewed. Experimental and modelling studies of the effect of pyrite on various processes related to the evolution of the repository environment and corrosion of the canister are also considered. The review has been limited to studies conducted for various national nuclear waste management programmes.

3.2 Characterisation and quantification of pyrite in bentonite and sedimentary host rocks

3.2.1 Pyrite in bentonite

The pyrite contents of a number of sources of bentonite have been reported. The pyrite content is estimated based on either an analysis of the sulphur content of the clay or on quantitative X-ray diffraction (XRD) analyses (Karnland 2010). The former method involves analysis of the total S content based on combustion at 1,200°C and analysis for sulphate based on a similar combustion at 800°C, the sulphide content then being given by the difference in the two values (Karnland 2010). Quantitative XRD analysis involves the fitting of the XRD patterns using commercial software. Based on the variability of the measured pyrite contents on duplicate samples reported by Karnland (2010), the reproducibility of both measurements may be as high as ±30–50%. Karnland et al. (2006) suggest an accuracy for XRD of ±1 wt.% suggesting that, in the case of pyrite, the XRD analyses should be considered semi-quantitative and that the combustion method provides a more reliable quantitative analysis.

Table 3-1 summarises the results of analyses of the pyrite content of various samples of bentonite from a number of sources reported by Karnland et al. (2006). Analyses are given for both combustion and XRD methods.

It is apparent from the data in Table 3-1 that the pyrite content of bentonite varies from deposit to deposit and even within a given deposit. The bentonite samples from the Czech Republic come from four different deposits, referred to as the Dnesice (Dn), Rokle (Ro), Zelena-Skalna (Sk), and Strance (St) deposits. Based on the results of the combustion analyses, these bentonites seem to contain little pyrite, which is confirmed by separate analyses of bentonite from the Rokle deposit which indicates an FeS_{2p} content of 0.00044 wt.% (Kolaříková et al. 2010). The three Danish and five Indian samples, taken from different locations within the respective deposits (Karnland et al. 2006), also show very little pyrite based on the combustion analyses.

In contrast to these bentonite sources, the samples from deposits in Germany (Friedland), Greece (Deponit CA-N) and the USA (MX-80) contain of the order of 0.5–1.0 wt.% pyrite (based on the combustion analyses). The pyrite contents shown in Table 3-1 are for replicate samples from the same batch of each material, indicating both sample-to-sample variability and the reproducibility of the measurement technique. Karnland et al. (2006) also report the results of XRD analyses of six batches of MX-80 bentonite received over a 20-year period, which showed the same mean pyrite content as the reference WyR1 material with a slightly larger standard deviation.

Table 3-1. Summary of pyrite analyses for various bentonites (Karnland et al. 2006).

Country of origin	Combustion		XRD	
	Bentonite sample	Pyrite content (wt.%)	Bentonite sample	Pyrite content (wt.%)
Czech Republic	RoR1	0.00	DnR1	0.8
	SkR1	0.06	RoR1	1.1
	StR1	0.00	SkR1	0.6
	StR1	0.00	StR1	0.9
Denmark	HoR1	0.00	HoR1	1.1
	RöR1	0.00	RöR1	1.0
	ÖlR1	0.96	ÖlR1	1.1
Germany	FrR1	0.62	FrR1a	1.4
	FrR1	0.71	FrR1b	0.9
	FrR1	0.69	FrR1c	1.7
	FrR1	0.65	Mean FrR1	1.3
	FrR1	0.74	Stand. Dev. FrR1	0.4
	Mean FrR1	0.68		
	Stand. Dev. FrR1	0.04		
Greece	MiR1	0.41	MiR1a	1.2
	MiR1	0.54	MiR1b	1.2
	MiR1	0.47	MiR1c	1.0
	MiR1	0.51	Mean MiR1	1.1
	MiR1	0.57	Stand. Dev. MiR1	0.1
	MiR1	0.38		
	Mean MiR1	0.48		
	Stand. Dev. MiR1	0.07		
India	Ku36R1	0.00	Ku36R1	0.9
	Ku37R1	0.00	Ku37R1	0.5
	Ku38R1	0.00	Ku38R1	0.5
	Ku39R1	0.00	Ku39R1	1.1
	Ku40R1	0.09	Ku40R1	0.3
USA	WyR1	0.24	WyR1a	0.5
	WyR1	0.30	WyR1b	0.6
	WyR1	0.08	WyR1c	0.6
	WyR1	0.26	Mean WyR1	0.6
	WyR1	0.31	s.d. WyR1	0.1
	Mean WyR1	0.24		
	s.d. WyR1	0.09		

The pyrite content of other types of bentonite that have or are being considered for buffer material in other national nuclear waste programmes include: 0.5–1.0 wt.% in the Japanese Kunigel-V1 (Ochs et al. 2004, Ohkubo et al. 2008), 0.7 wt.% in German Volclay KWK (Van Loon et al. 2007), and 0.02 wt.% in the ENRESA-supplied bentonite for the FEBEX experiment (Fernández et al. 2004).

Although there have been a significant number of analyses of the amount of FeS_{2p} in bentonite, there is little information concerning the nature of the pyrite. The fact that pyrite can be detected by XRD indicates the presence of crystalline material, but there is little information about the size or shape of the FeS_{2p} particles. Figure 3-1 shows a photograph of a Wyoming bentonite thin section that was subjected to synchrotron-based XRD (S-µXRD, Lange et al. 2010) and which contains a small pyrite particle (spot T1.2) that was specifically identified by the S-µXRD technique.

Fukushi et al. (2010) characterised unprocessed bentonite deposits from the Zao region in Japan. Of the three samples examined, pyrite was observed in only one, in the form of greenish veins surrounding bentonite particles. The pyrite was present as well-defined, faceted crystals with a size of 20–25 µm (Figure 3-2), and was believed to have been formed during exposure to an aqueous phase at a temperature < 100°C, implying formation of FeS_{2p} via a dissolution-precipitation process involving various iron sulphides rather than via a high-temperature melt. Several of the bentonite deposits examined by Karnland et al. (2006) are also thought to have been formed by exposure to marine or aqueous environments, again implying pyrite formation via a dissolution-precipitation process.

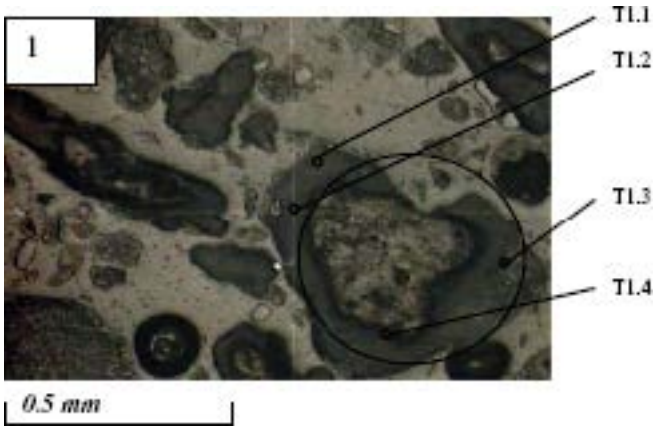

Figure 3-1. *Photograph of bentonite thin section used for synchrotron micro X-ray diffraction (Lange et al. 2010). Spot T1.2 was identified as pyrite.*

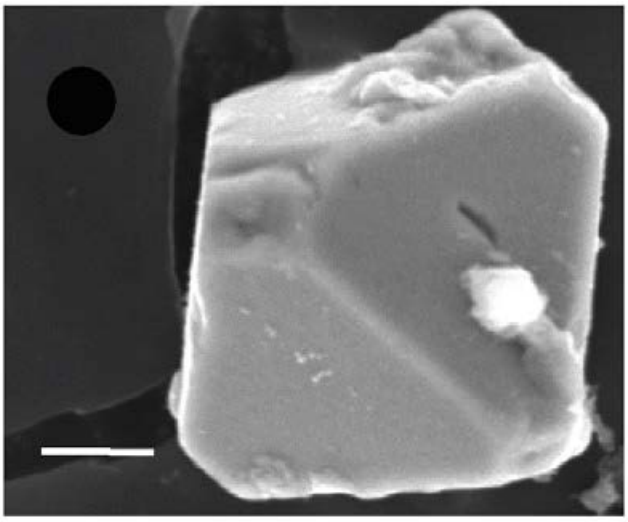

Figure 3-2. *Euhedral pyrite particle in Japanese unprocessed bentonite deposit (Fukushi et al. 2010). The scale bar is 5 µm long.*

3.2.2 Pyrite in sedimentary host rocks

Pyrite is also a significant component of several sedimentary host rock formations considered for nuclear waste repositories in various countries. Because of their potential significance on the performance of the respective repositories, these pyrite inclusions have been characterised in some detail. For example, the pyrite content of Opalinus Clay is ~1 wt.% (Nagra 2002). Techer et al. (2009) describe the presence of framboids and discrete crystals of pyrite, which showed evidence for oxidation during long-term experiments in the Mont Terri URL and during storage in the laboratory. (Framboids are spherical agglomerations of pyrite particles with an appearance similar to a raspberry, the French word for which is framboise). Upon oxidation, these particles became covered by a layer of calcium sulphate.

The Belgian Boom Clay contains up to 9 wt.% pyrite (Delécaut 2004, Zhang et al. 2008). The pyrite takes a number of forms, including large concreted nodules of several cm in dimension, to smaller aggregates, and framboidal particles and discrete crystals (Figure 3-3, Delécaut 2004).

3.3 Experimental studies of the behaviour of pyrite in bentonite

Although pyrite is expected to have a number of impacts on the repository environment, there have been few experimental studies of these processes using bentonite samples. Similar to the observation of the oxidation of pyrite in Opalinus Clay reported by Techer et al. (2009), Kolaříková et al. (2010) observed the formation of gypsum ($CaSO_4 \cdot 2H_2O$) when Rokle bentonite was exposed to hydrothermal conditions at temperatures up to 100°C for a period of 45 months. The appearance of gypsum was interpreted as being the result of the oxidation of pyrite in the bentonite or present in graphite added to the experiment to improve the heat transfer characteristics. In contrast Melamed and Pitkänen (1994, 1996) observed a decrease in the amount of gypsum following exposure of bentonite to water at 75°C for periods of up to 36 months, believed to be due to dissolution and ion-exchange of Ca^{2+} by the MX-80 bentonite. More interestingly, the authors observed the development of concentric rings of reddish-brown corrosion products on pyrite particles in the bentonite, identified by XRD to contain goethite and siderite (Figure 3-4).

Lazo et al. (2003) studied the redox properties of bentonite-NaCl solution slurries, specifically the consumption of dissolved O_2. Two types of bentonite were used, MX-80 containing 0.3 wt.% pyrite and Montigel containing very little. Despite the differences in pyrite content of the two clays, the rate of O_2 consumption was similar, leading the authors to conclude that the oxidation of pyrite may not be a major contributor to the consumption of the initially trapped oxygen in a repository.

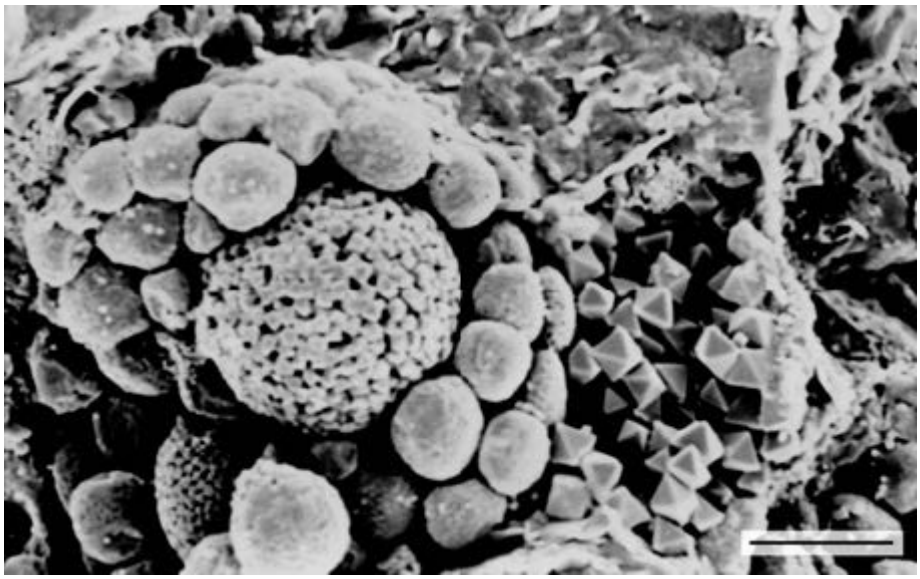

Figure 3-3. *Framboidal and discrete particulate pyrite in Boom Clay (Delécaut 2004). The scale bar is 10 µm.*

Figure 3-4. *Oxidised pyrite particle in MX-80 bentonite (after Melamed and Pitkänen 1994). The diameter of the oxidised particle is approximately 800 µm.*

3.4 Modelling studies of the behaviour of pyrite under repository conditions

In contrast to the small number of experimental studies of the behaviour of pyrite in bentonite, there have been a large number of modelling studies related to the effect of pyrite on canister corrosion, the consumption of O_2, and changes in the mineralogy and other properties of the bentonite buffer.

3.4.1 Canister corrosion

In the SR-Site safety assessment, it is assumed that pyrite dissolution can lead to the corrosion of the canister (SKB 2010a). For pyrite in the buffer, the extent of corrosion is estimated based on both mass-balance and mass-transport arguments. For the mass-balance argument, it is conservatively assumed that each pyrite molecule will dissolve to form two sulphide molecules which in turn will support the corrosion of four Cu atoms

$$4Cu + FeS_{2p} + 4H_2O + 2e^- \rightarrow 2Cu_2S + Fe^{2+} + 2H_2 + 4OH^- \quad (3\text{-}1)$$

Whilst this reaction is mass balanced, it is not electron balanced since pyrite is a polysulphide rather than a sulphide. Regardless, the maximum depth of corrosion to the sides of the canister based on this approach is predicted to be 0.1 mm and 0.9 mm for MX-80 and Ibeco-RWC bentonites, respectively (SKB 2010a). (The pyrite contents of MX-80 and Ibeco-RWC bentonites are assumed to be 0.07 wt.% and 0.5 wt.%, respectively). If the limited solubility of pyrite and the low diffusivity of HS^- are taken into account, only the pyrite within 2 cm of the canister surface will contribute to corrosion over a 10^6 timescale, resulting in 1 µm of corrosion for the reference values of the solubility and diffusivity (SKB 2010a).

King et al. (2011a, b) have developed a detailed reactive-transport model for predicting the extent of corrosion of the canister due to HS^- from various sources, including pyrite dissolution, microbial sulphate reduction, and the ground water itself. In the Copper Sulphide Model (CSM), pyrite is assumed to both react with O_2 during the aerobic phase, according to

$$FeS_{2p} + 3.75O_2 + 3.5H_2O \rightarrow Fe(OH)_3 + 2SO_4^{2-} + 4H^+ \quad (3\text{-}2)$$

and to dissolve under anaerobic conditions to release sulphide, according to

$$FeS_{2p} + 0.75H_2O \rightarrow Fe(II) + 1.5HS^- + 0.25S_2O_3^{2-} \quad (3\text{-}3)$$

The assumption that the dissolution of pyrite results in the formation of both HS^- and thiosulphate ions is based on the study of the disproportionation of polysulphide in aqueous solutions (Licht and Davis 1997). Simulations using the CSM predict long-term corrosion rates due to all sources of sulphide of the order of < 1 nm/year, of the same order of magnitude as those predicted in for the SR-Site safety assessment (SKB 2010a). More importantly, of the different sources of sulphide, pyrite dissolution is predicted to account for < 5% of the total amount of corrosion (King et al. 2011b).

3.4.2 Oxygen consumption

In common with other nuclear waste management programmes, SKB has considered the impact of the oxidation of pyrite on the consumption of the initially trapped O_2 in the repository (Grandia et al. 2006, Puigdomenech et al. 2000, 2001, Sidborn and Neretnieks 2003, Wersin et al. 1994). The stoichiometry of the reaction between FeS_{2p} and O_2 is typically given by Reaction (3-2). The reaction has been assumed to be both abiotic in nature (e.g., Grandia et al. 2006) or microbially mediated (e.g., Sidborn and Neretnieks 2003). Predictions of the time to consume the initially trapped O_2 range from a few months (Grandia et al. 2006) to as long as 300 years (Wersin et al. 1994), although these predictions are inconsistent with the experimental observations of Lazo et al. (2003) discussed above who observed no apparent effect of pyrite content of bentonite on the rate of O_2 consumption.

Zhang et al. (2008) describe a numerical model to predict the evolution of Boom Clay subject to heating, irradiation, and microbial activity. Pyrite dissolution *and* precipitation were described by the reaction

$$FeS_{2p} + H_2O + 3.5O_2 = Fe^{2+} + 2SO_4^{2-} + 2H^+ \quad (3\text{-}4)$$

although there is no evidence to suggest that this reaction is reversible and the fact that the oxidation of S_2^{2-} to SO_4^{2-} (and the reverse process) involves the transfer of an average of seven electrons per S atom makes the reversibility of this reaction extremely unlikely. Zhang et al. (2008) suggested an equilibrium constant for Reaction (3-4) of $10^{224.64}$ at 16.5°C, which implies that the reaction would be well over to the right-hand side, regardless of any questions regarding the kinetics of the reduction process. Nevertheless, little net pyrite dissolution or precipitation was predicted to occur in Boom Clay subject to either heating alone or heating and irradiation. In order to predict the precipitation of pyrite that was observed in the CERBERUS experiment at the HADES facility in Mol, Belgium, Zhang et al. (2008) extended their model to include a microbial component. The activity of both iron-reducing (IRB) and sulphate-reducing bacteria (SRB) was incorporated into the model, along with an additional process for the dissolution/precipitation of pyrite

$$Fe^{2+} + 2HS^- + 0.5O_2 = FeS_{2p} + H_2O \quad (3\text{-}5)$$

although the basis for this reaction is unclear since pyrite is not formed under oxic conditions. With the inclusion of this reaction and the IRB and SRB microbial activity, however, Zhang et al. (2008) were able to predict the precipitation of FeS_{2p}, in apparent agreement with experimental observations.

3.4.3 Impact on processes in the buffer and host rock under anaerobic conditions

There have been a number of attempts to include the effect of pyrite on the evolution of the bentonite and far-field under anaerobic conditions. Arcos et al. (2008) suggested that the redox potential in the bentonite in a KBS-3 repository is close to that in the granitic ground water, which in turn appears to be close to equilibrium with pyrite and siderite.

In the French nuclear waste management programme, the reactive-transport code KIRMAT has been used to predict the alteration of bentonite (Marty et al. 2010), transport and reactions in the bentonite (Montes-H et al. 2005a, b), and cation exchange (Montes-H et al. 2005c). The dissolution rate of a mineral m (v_{dm}^s) in the KIRMAT code is treated using a generalised expression of the form

$$v_{dm}^s = k_{dm}^{pH} S_m^{eff} a_{H^+}^n \left(1 - \frac{Q_m}{K_m}\right) \quad (3\text{-}6)$$

where k_{dm}^{pH} is a pH-dependent dissolution rate constant, S_m^{eff} is the effective surface area of the mineral, $a_{H^+}^n$ is the activity of H^+ ions in solution and the value of the exponent n is typically positive in acid solution, zero at neutral pH and negative in basic solution, and Q_m and K_m are the ion activity product and the equilibrium constant, respectively. The reaction for the dissolution of pyrite is not given, but an equilibrium constant of $10^{-67.89}$ at 100°C is quoted (Marty et al. 2010, Montes-H et al. 2005a, b, c). Furthermore, the value given for the dissolution rate constant is (i) independent of pH, (ii) used by Marty et al. (2010) to predict the rate of both pyrite dissolution and precipitation, and (iii) appears to have been taken from a literature study of the oxidative dissolution of pyrite, despite the modelling being conducted under supposed anaerobic conditions. In a separate study using the CRUNCH reactive-transport code, Bildstein et al. (2006) have also used an apparent oxidative dissolution rate constant to describe the dissolution and precipitation of pyrite under anaerobic conditions when modelling iron-bentonite interactions in a French repository.

4 Aqueous chemistry of sulphides and polysulphides

4.1 Speciation of dissolved sulphide

The dissociation of dissolved H_2S in aqueous solution occurs in two stages

$$H_2S \Leftrightarrow HS^- + H^+ \qquad K_1 = \frac{\{HS^-\}\{H^+\}}{\{H_2S\}} \tag{4-1a}$$

and

$$HS^- \Leftrightarrow S^{2-} + H^+ \qquad K_2 = \frac{\{S^{2-}\}\{H^+\}}{\{HS^-\}} \tag{4-1b}$$

where the curly brackets denote activity. The value of K_1 is well characterised and at infinite dilution has a value of $10^{-6.98\pm0.03}$ at 25°C and 1 bar pressure (Rickard and Luther 2007). The value of K_2 is less well characterised since the formation of polysulphides at alkaline pH complicates its measurement. The best estimate for pK_2 is > 18 (Rickard and Luther 2007). Figure 4-1 shows the predicted distribution of sulphide species based on Reactions (4-1a) and (4-1b) with pK_1 and pK_2 values of –6.98 and –18, respectively, for a total dissolved sulphide concentration of 10^{-5} mol·dm^{-3}, similar to that in the ground water at Forsmark. It is important to note that S^{2-} is virtually non-existent in aqueous solution.

The temperature dependence of pK_1 at infinite dilution is given by (Rickard and Luther 2007)

$$pK_1 = -98.080 + 5765.4/T + 15.0455 \ln T \tag{4-2}$$

where T is the temperature in K. Rickard and Luther (2007) also provide the dependence of pK_1 on salinity (for seawater).

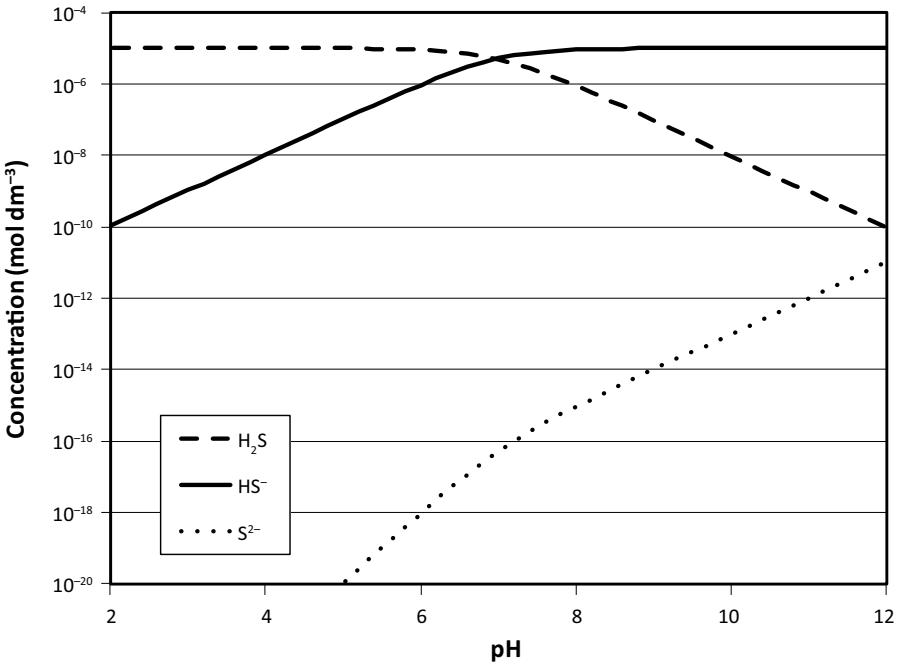

Figure 4-1. *Concentrations of H_2S, HS^-, and S^{2-} for a total dissolved sulphide concentration of 10^{-5} mol·dm^{-3}.*

4.2 Speciation of dissolved polysulphides

Polysulphide ions consist of a chain of sulphur atoms attached to a sulphide ion in the general form S_n^{2-} (Rickard and Luther 2007). Polysulphides with n values of 2–8 have been characterised by Kamyshny et al. (2004). Polysulphide species dissociate in aqueous solution in an analogous fashion to the sulphides

$$H_2S_n \Leftrightarrow HS_n^- + H^+ \qquad K_1' = \frac{\{HS_n^-\}\{H^+\}}{\{H_2S_n\}} \tag{4-3a}$$

and

$$HS_n^- \Leftrightarrow S_n^{2-} + H^+ \qquad K_2' = \frac{\{S_n^{2-}\}\{H^+\}}{\{HS_n^-\}} \tag{4-3b}$$

In (alkaline) aqueous solution in the presence of excess S(0), the predominant polysulphide species are (in order of decreasing concentration): S_5^{2-}, S_6^{2-}, S_4^{2-}, S_7^{2-}, S_3^{2-}, S_8^{2-}, and S_2^{2-} (Kamyshny et al. 2004, Rickard and Luther 2007). The species HS_2^- is the most-predominant protonated species over a wide range of pH and is the predominant polysulphide species at pH ≤ 7. Figure 4-2 shows the distribution of sulphide and polysulphide species as a function of pH (Rickard and Luther 2007). The HS^- ion is the predominant dissolved species up to ~pH 9.5, with the various un-protonated polysulphides becoming increasingly dominant at higher pH. At pH 7 the ratio of the total polysulphide concentration to the concentration of HS^- is ~0.01.

Polysulphide ions will also participate in redox reactions involving various oxidised sulphur species, such as sulphate

$$S_2^{2-} + H_2O = 1.75HS^- + 0.25SO_4^{2-} + 0.25H^+ \tag{4-4}$$

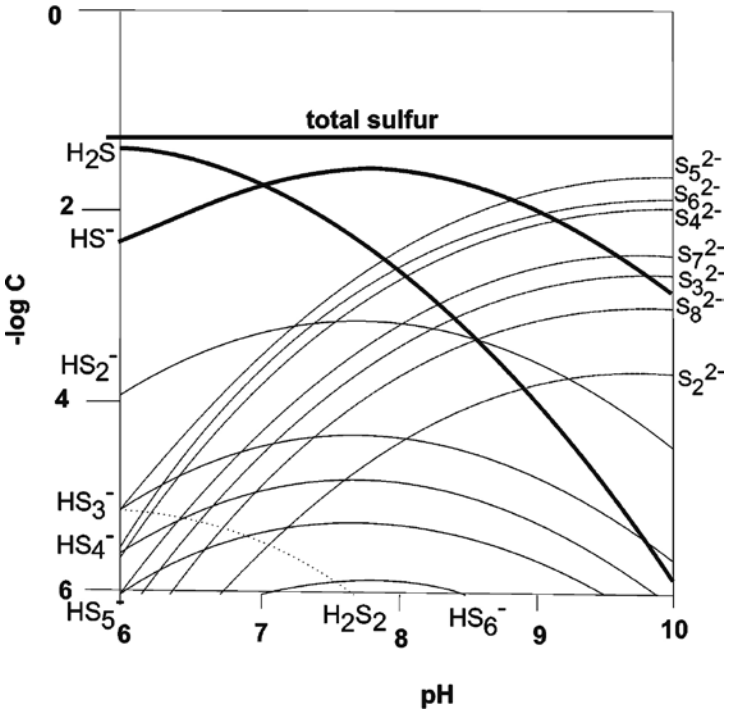

Figure 4-2. *Distribution of sulphide and polysulphide species as a function of pH in the presence of excess S(0) for a total dissolved sulphur concentration of $5 \cdot 10^{-2}$ mol·dm^{-3} (Rickard and Luther 2007).*

Figure 4-3 shows the distribution of sulphide, polysulphide, and sulphate as a function of redox potential for various pH values and a total dissolved sulphur concentration of 10^{-3} mol·dm^{-3} (Rickard and Luther 2007). It is interesting to note that, in the absence of elemental sulphur, the bisulphide species HS_2^- and S_2^{2-} are predicted to be more stable than the higher polysulphides. Furthermore, at pH 8 (i.e., close to the pH of bentonite pore water), the ratio of the concentration of HS^- to that of either HS_2^- or S_2^{2-} is > 10^{10} at the E_h corresponding to the H_2/H_2O equilibrium line, suggesting that HS^- will dominate the speciation of dissolved sulphide and polysulphide under anaerobic conditions.

4.3 Dissolved iron-sulphur species

Sulphide will also form complexes with Fe(II) ions in solution. A range of possible dissolved Fe-S complexes and clusters is described by Rickard and Luther (2007), including: $Fe(HS)^+$, $Fe(HS)_2$, $Fe(HS)_3^-$, $Fe_2(HS)^{3+}$, $Fe_3(HS)^{5+}$, FeS_4, $Fe_2S_4^{2+}$, FeS_5, $Fe_2S_5^{2+}$, FeS, and Fe_2S_2. The relative abundance of these species depends on pH and the relative Fe^{2+} and HS^- concentrations, but they tend to be more predominant in HS^- rich environments. Further discussion of the stability and distribution of these species can be found in Rickard and Luther (2007).

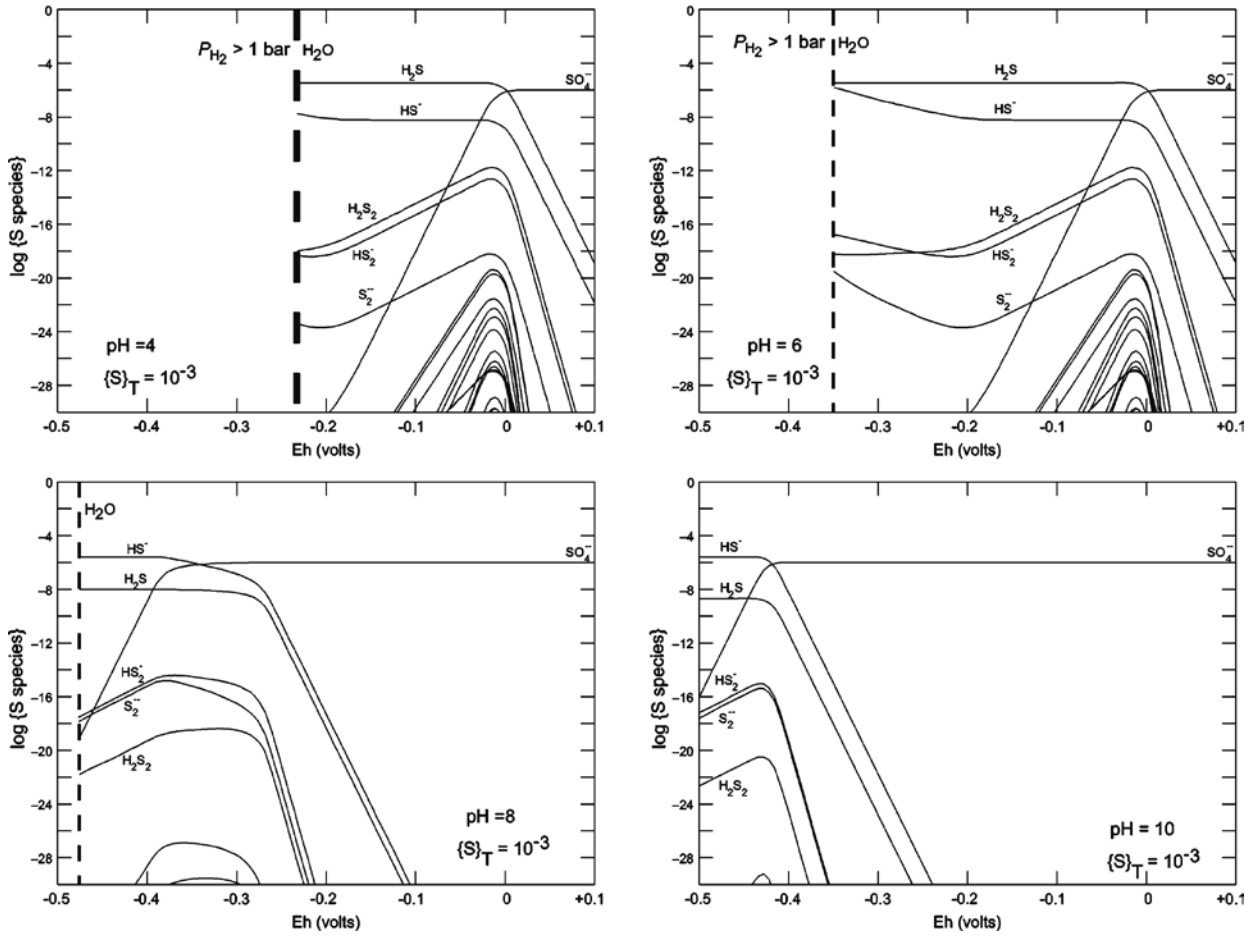

Figure 4-3. *Distribution of sulphide and polysulphide species and sulphate as a function of redox potential at various pH for a total dissolved sulphur concentration of 10^{-3} mol·dm^{-3} (Rickard and Luther 2007).*

5 Solubility of pyrite and other iron sulphides

As a general rule, iron sulphides are relatively insoluble, especially under the redox conditions and pH expected in the repository. For this reason, there are few experimental studies of the solubility of the more stable iron sulphides in the literature, and none at all for pyrite. As an alternative to measuring the solubility experimentally, the solubility product can be estimated from the free energy change for an assumed dissolution process. The validity of this latter approach has been demonstrated for mackinawite and greigite, for which experimental solubility measurements are available. The solubility data for mackinawite and greigite are discussed first before extending the thermodynamic approach to the prediction of the solubility of pyrite.

5.1 Mackinawite and greigite

The solubility of FeS_m has been measured by a number of workers, including recently by Rickard (2006). Earlier studies have been reviewed by Davison (1991). Rickard (2006) found that the solubility of FeS_m (expressed in terms of the concentration of dissolved Fe(II)) exhibited a pH-dependent region at pH < 6–8 (depending on sulphide concentration) and a pH-independent region at higher pH. In the "low-pH" region, dissolution of mackinawite could be described by

$$FeS_m + 2H^+ \rightarrow Fe^{2+} + H_2S \quad (5\text{-}1)$$

In the "high-pH" region, the stable aqueous species was considered to be dissolved FeS^0. The overall solubility could be expressed as (Rickard 2006)

$$\log \sum [\text{Fe(II)}] = \log K_0 + \log K^*_{sp,1} - \log \{H_2S\} - 2\text{pH} \quad (5\text{-}2)$$

where K_0 is the intrinsic solubility of FeS_m ($\log K_0 = -5.7$) and $K^*_{sp,1}$ is the solubility product for Reaction (5-1)

$$K^*_{sp,1} = \frac{\{Fe^{2+}\}\{H_2S\}}{\{H^+\}^2} \quad (5\text{-}3)$$

and has a value of $10^{3.5\pm0.25}$ at 23°C.

Figure 5-1 shows a comparison of some of the measured total sulphide concentrations of Rickard (2006) and predicted H_2S or HS^- concentrations (or, more strictly, activities) calculated on the basis of the equilibrium expression for Reaction (5-1) (for pH < 7) and the corresponding reaction involving HS^- (for pH ≥ 7), namely:

$$FeS_m + H^+ = Fe^{2+} + HS^- \quad (5\text{-}4)$$

The free energies of formation used for the various species are given in Table 5-1 and the free energy change for various reactions are given in Table 5-2.

For this comparison, data were selected from the study of Rickard (2006) with dissolved Fe(II) concentrations close to 10^{-4}, 10^{-6}, or 10^{-8} mol·dm^{-3} and the corresponding measured total sulphide concentrations were then plotted on the figure. Good agreement is found between measured and predicted sulphide concentrations suggesting that the solubility of mackinawite can be reasonably predicted based on the available thermodynamic data. As noted above, however, Rickard (2006) reported that the solubility of mackinawite was independent of pH in alkaline solution (pH > 8) so that the thermodynamic prediction is likely to be less reliable at elevated pH.

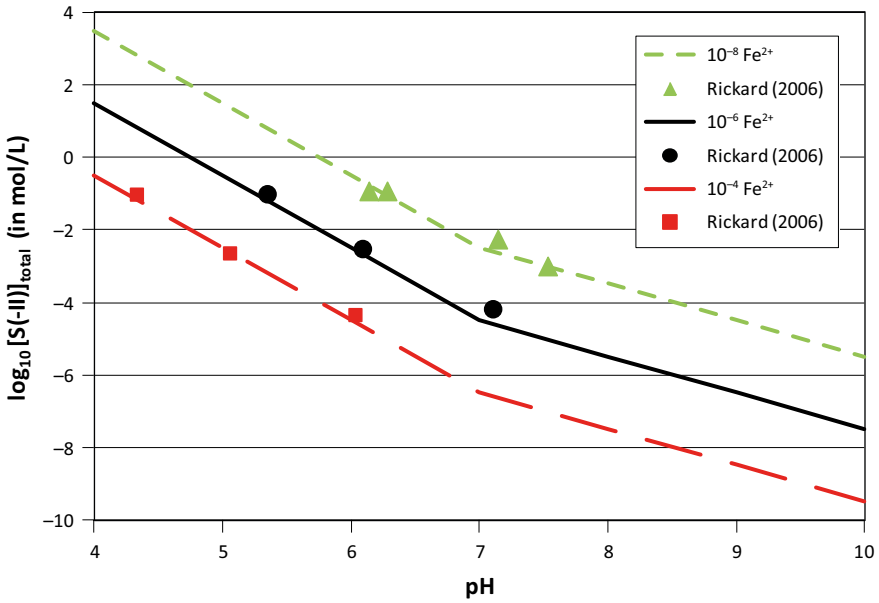

Figure 5-1. *Comparison of the pH dependence of the measured total sulphide concentration from Rickard (2006) and predicted activities of H_2S or HS^- for the dissolution of mackinawite for dissolved Fe(II) concentrations of 10^{-4}, 10^{-6}, and 10^{-8} mol·dm^{-3}. The predicted concentrations are calculated from Reaction (5-1) for pH < 7 and Reaction (5-4) for pH ≥ 7.*

Table 5-1. Summary of free energy of formation data used in solubility calculations.

Species	ΔG_f^0 (kJ/mol)	Reference
Mackinawite FeS_m	–98.38	Inferred from Rickard 2006
Greigite Fe_3S_{4g}	–308.30	Rickard and Luther 2007
Pyrite FeS_{2p}	–160.229	Robie et al. 1978
Fe^{2+}	–90.53	Rickard and Luther 2007
$H_2S(aq)$	–27.83	Wagman et al. 1982
HS^-	12.05	Rickard and Luther 2007
HS_2^-	22.07	Rickard and Luther 2007

Table 5-2. Free energy of reaction used in solubility calculations.

Reaction	ΔG_r^0 (kJ/mol)
$FeS_m + 2H^+ = Fe^{2+} + H_2S$	–19.98
$FeS_m + H^+ = Fe^{2+} + HS^-$	19.90
$Fe_3S_{4g} + 6H^+ = 3Fe^{2+} + 3H_2S + S^0$	–46.78
$Fe_3S_{4g} + 3H^+ = 3Fe^{2+} + 3HS^- + S^0$	72.86
$FeS_{2p} + 2H^+ = Fe^{2+} + H_2S + S^0$	41.87
$FeS_{2p} + H^+ = Fe^{2+} + HS^- + S^0$	81.75
$FeS_{2p} + H^+ = Fe^{2+} + HS_2^-$	91.77

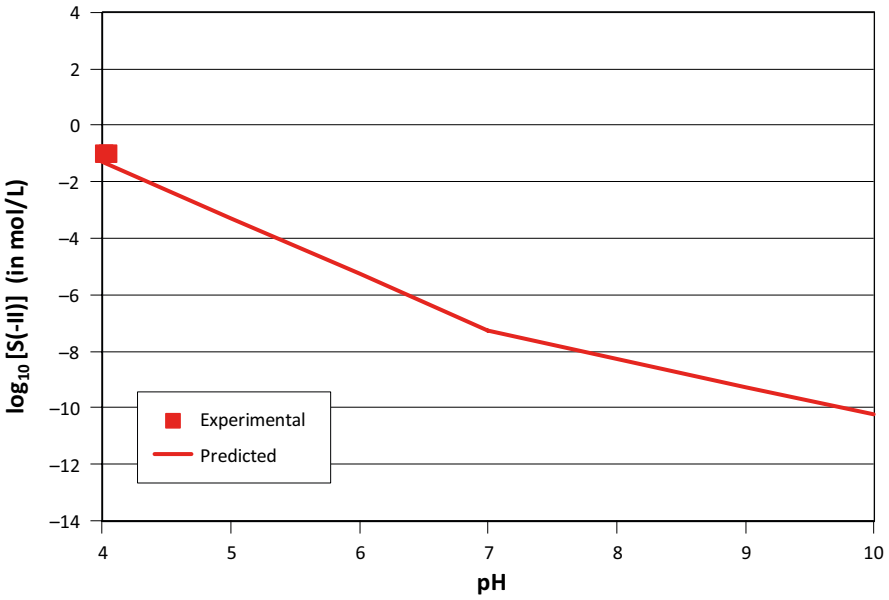

Figure 5-2. *Comparison of the experimental and predicted activities of H_2S (for pH < 7) or HS^- (for pH ≥ 7) for the solubility of greigite for a dissolved Fe(II) concentration of 10^{-4} mol·dm^{-3}. The experimental data point is taken from Rickard and Luther (2007), calculated from the original study of Berner (1967). The predicted concentrations are calculated from Reaction (5-5a) for pH < 7 and Reaction (5-5b) for pH ≥ 7.*

Rickard and Luther (2007) report only a single experimental measurement of the solubility of greigite, that by Berner (1967). Figure 5-2 shows a similar comparison of measured and thermodynamically predicted sulphide concentrations as a function of pH for the dissolution of greigite. In this case, Fe_3S_{4g} is assumed to dissolve with the formation of sulphide and elemental sulphur S^0

$$Fe_3S_{4g} + 6H^+ = 3Fe^{2+} + 3H_2S + S^0 \quad (5\text{-}5a)$$

and

$$Fe_3S_{4g} + 3H^+ = 3Fe^{2+} + 3HS^- + S^0 \quad (5\text{-}5b)$$

As for the solubility of mackinawite, there is reasonable agreement between the thermodynamically predicted sulphide concentration for the dissolution of greigite and that derived from the experimental study of Berner (1967), albeit only for a single experimental data point for comparison.

5.2 Pyrite

Having established the principle of using thermodynamics to predict the solubility of mackinawite and greigite, we now extend the method to the prediction of the solubility of pyrite for which there are no experimental measurements. For this purpose, we consider both the dissolution of FeS_{2p} to produce sulphide and elemental sulphur

$$FeS_{2p} + 2H^+ = Fe^{2+} + H_2S + S^0 \quad (5\text{-}6a)$$

and

$$FeS_{2p} + H^+ = Fe^{2+} + HS^- + S^0 \quad (5\text{-}6b)$$

and the dissolution of pyrite to produce ferrous and polysulphide ions

$$FeS_{2p} + H^+ = Fe^{2+} + HS_2^- \quad (5\text{-}7)$$

Figure 5-3 shows the predicted concentration of sulphide in equilibrium with pyrite in the presence of elemental sulphur for dissolved Fe^{2+} concentrations of 10^{-4}, 10^{-6}, and 10^{-8} mol·dm^{-3} based on Reactions (5-6a) and (5-6b) for pH < 7 and pH ≥ 7, respectively.

Predicting the concentration of sulphide as a function of Fe^{2+} concentration is appropriate if the solubility of some other Fe(II) phase controls the dissolved Fe(II) concentration. However, since pyrite is likely to be the least-soluble Fe(II) solid present, it is reasonable to assume that dissolution of FeS_{2p} will control the dissolved [Fe^{2+}], in which case we need to consider the congruent dissolution of pyrite. Figure 5-4 shows the predicted sulphide or polysulphide concentrations as a function of pH for the congruent dissolution of pyrite for Reactions (5-6a), (5-6b), and (5-7). Because the pyrite is dissolving congruently, the dissolved Fe^{2+} concentration also varies with pH and is equal to the concentration of H_2S, HS^-, or HS_2^-. Thus, depending upon the precise dissolution pathway, the concentration of sulphide or polysulphide in bentonite pore water (assumed to be pH 8) is predicted to be of the order of $10^{-11.2}$ to $10^{-12.0}$ mol·dm^{-3} at 25°C.

As noted above, the solubility of FeS_{2p} is too low to measure at ambient temperature. Ohmoto et al. (1994) measured the solubility of pyrite in NaCl solutions at temperatures of 250–350°C. Their data seem to indicate an increase in solubility by as much as two orders of magnitude over this range of temperature, although there is a lot of scatter in the data and the authors themselves concluded that the solubility of FeS_{2p} and of other iron sulphides is relatively insensitive to temperature.

The solubility of pyrite is significantly lower than that for mackinawite or greigite. Figure 5-5 shows a comparison of the predicted HS^- activity based on Reactions (5-1) and (5-4) for mackinawite, Reactions (5-5a) and (5-5b) for greigite, and Reactions (5-6a) and (5-6b) for pyrite for a dissolved Fe^{2+} concentration of 10^{-6} mol·dm^{-3}. Based on this comparison, the concentration of HS^- is a factor of approximately 10 orders of magnitude lower for pyrite than for either of the other two iron sulphides.

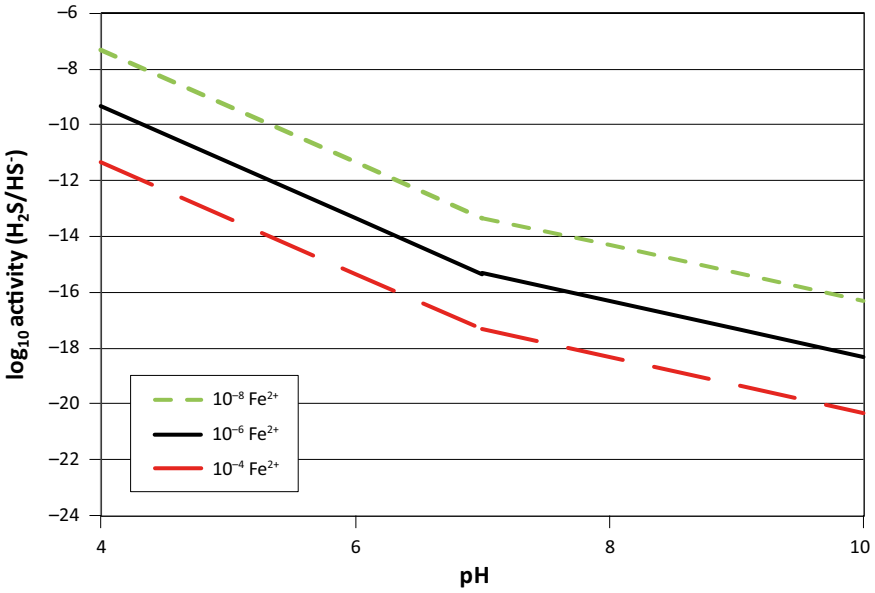

Figure 5-3. *Predicted activities of H_2S or HS^- for the solubility of pyrite with the formation of elemental sulphur for dissolved Fe(II) concentrations of 10^{-4}, 10^{-6}, and 10^{-8} mol·dm^{-3}.*

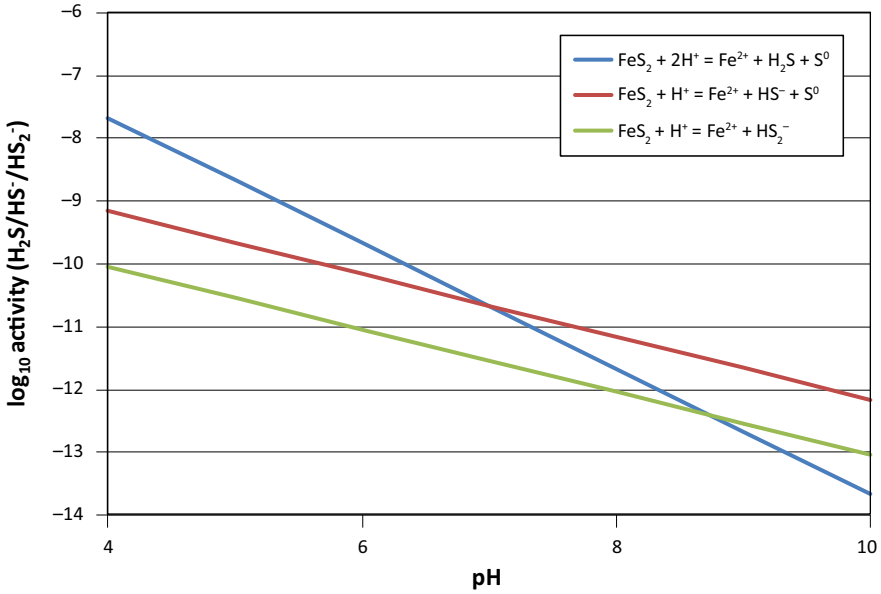

Figure 5-4. *Predicted activities of H_2S, HS^-, or HS_2^- for the congruent dissolution of pyrite.*

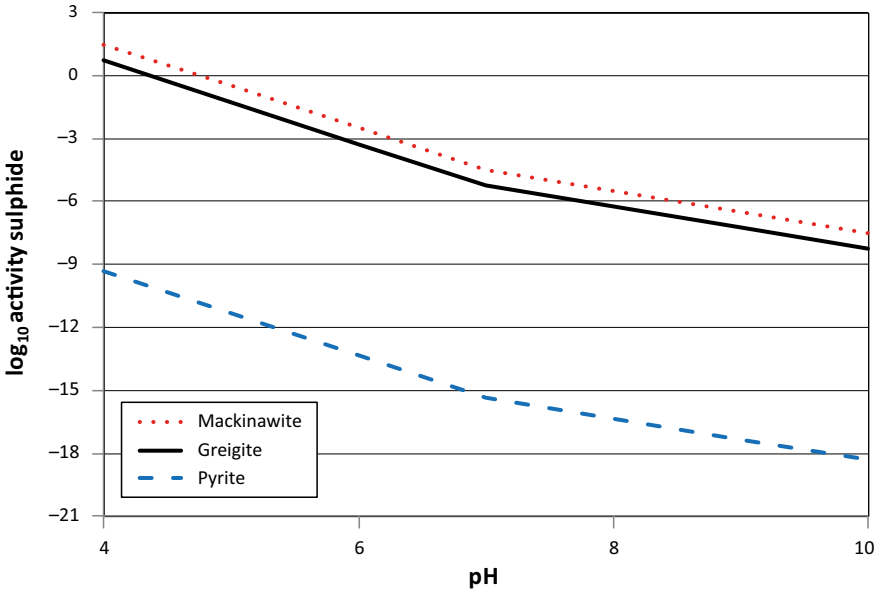

Figure 5-5. *Comparison of the predicted sulphide activity for the dissolution of mackinawite, greigite, and pyrite based on Reactions (5-1) and (5-4), (5-5a) and (5-5b), and (5-6a) and (5-6b), respectively. Dissolved Fe^{2+} concentration of 10^{-6} mol·dm^{-3}. For each iron sulphide, the first of the two noted reactions was used for pH values < 7 and the second noted reaction for pH ≥ 7. At pH < 7, the dissolved sulphide is present as H_2S, with HS^- predominant at pH ≥ 7.*

6 Pyrite dissolution and electrochemistry

The dissolution of pyrite can occur oxidatively, reductively, or congruently with no change in oxidation state. These different mechanisms are distinguished by the change, if any, in the oxidation state of the sulphur species. Oxidative dissolution is characterised by the oxidation of sulphur from the average –I oxidation state in FeS_{2p} to SO_4^{2-} (a net transfer of seven electrons from S_2^{2-}), although other stable intermediate oxidation states are also formed under some circumstances. Reductive dissolution is defined here as involving the reduction of S_2^{2-} to two S^{2-} species (a net transfer of one electron). Finally, congruent dissolution is defined as the dissolution of FeS_{2p} as Fe^{2+} and S_2^{2-}, with possible subsequent disproportionation of the dissolved polysulphide species.

Of these three dissolution pathways, those of most interest here are the reductive and congruent dissolution routes. Although oxidative dissolution is not the main focus of the current review, the mechanism is briefly summarised here because of the impact of the oxic phase on the subsequent behaviour during the anaerobic period.

6.1 Oxidative dissolution

The oxidative dissolution of pyrite is involved in a number of important industrial and environmental processes, including: mineral flotation and leaching, desulphurisation of coal, and acid rock (or mine) drainage (Chandra and Gerson 2010, Langmuir 1997, Rickard and Luther 2007, Rimstidt and Vaughan 2003, Vaughan 2005). Although the oxidative dissolution process can be accelerated by microbial activity, the predominant underlying processes are electrochemical in nature, with the mechanism and rate of dissolution primarily determined by potential and the (semi-conducting) properties of the pyrite, as well as the pH, temperature, the nature and concentration of the oxidant, hydrodynamic conditions, grain size, the surface area:volume ratio, and pressure (Chandra and Gerson 2010).

The two most important oxidants for pyrite are O_2 and Fe^{3+}. The overall stoichiometry of the respective dissolution processes are (Vaughan 2005)

$$FeS_{2p} + 3.5O_2 + H_2O \rightarrow Fe^{2+} + 2SO_4^{2-} + 2H^+ \quad (6\text{-}1a)$$

and

$$FeS_{2p} + 14Fe^{3+} + 8H_2O \rightarrow 15Fe^{2+} + 2SO_4^{2-} + 16H^+ \quad (6\text{-}1b)$$

Although ferric species are important intermediates of the oxidation process and are occasionally described as products of the overall reaction, the general consensus is that oxidative dissolution under acidic conditions produces Fe^{2+} species. The species undergoing oxidation, therefore, is the disulphide S_2^{2-}, with sulphate the predominant product, although some researchers report various stable intermediate sulphur oxyanions, such as thiosulphate $S_2O_3^{2-}$, polythionates $S_nO_6^{2-}$, and sulphite SO_3^{2-} (Chandra and Gerson 2010, Moses et al. 1987). Precipitated Fe(III) corrosion products are reported in neutral and alkaline solutions (Caldeira et al. 2003, 2010, Huminicki and Rimstidt 2009, Todd et al. 2003), in which dissolved Fe(II) is more readily oxidised homogeneously to Fe(III) by O_2.

The multiple electron transfer steps involved in the oxidation of S_2^{2-} occur sequentially at the anodic sites on the pyrite surface. Based on the results of experiments using isotopically labelled H_2O and O_2, it has been shown that the oxygen atoms in the eventual SO_4^{2-} (or sulphur oxyanion) product derive from H_2O, whereas the O_2 participates in the cathodic process and can be found in precipitated iron oxyhydroxides (Heidel and Tichomirowa 2010, Usher et al. 2004). This is evidence for anodic and cathodic processes occurring on physically separated sites.

The sequence of electron transfers involved in the oxidation of the S sites (and the addition of oxygen from H_2O) can be represented by (after Rimstidt and Vaughan 2003)

$$\begin{array}{l} \mathrm{py-S-S \rightarrow py-S-S^{+} + e^{-} \xrightarrow{+H_2O} py-S-SOH + H^{+} \longrightarrow py-S-SO + H^{+} + e^{-}} \\ \qquad\qquad\qquad\qquad\qquad\qquad\qquad\qquad\qquad\qquad\qquad\qquad \downarrow \\ \mathrm{py-S-SO_2 + H^{+} + e^{-} \longleftarrow py-S-SO_2H + H^{+} \xleftarrow{+H_2O} py-S-SO^{+} + e^{-}} \\ \qquad \downarrow \\ \mathrm{py-S-SO_2^{+} + e^{-} \xrightarrow{+H_2O} py-S-S-O_3H + H^{+} \longrightarrow py-S-SO_3 + H^{+} + e^{-}} \end{array} \qquad (6\text{-}2)$$

where py-S-S represents a polysulphide species at the pyrite (py) surface. This sequence represents a series of electron transfer, hydrolysis, and deprotonation steps.

The surface intermediate py-S-SO_3 is a key species in the sequential oxidation process. In alkaline conditions or in anoxic Fe^{3+} solutions (Moses et al. 1987), the py-S bond can cleave and thiosulphate $S_2O_3^{2-}$ is observed in solution. In the presence of either O_2 or Fe^{3+}, especially in acidic solution, the surface intermediate is further oxidised all the way to sulphate, which, following cleavage of the S-S bond, is the only sulphur oxyanion observed in solution

$$\begin{array}{l} \mathrm{py-S-SO_3 \rightarrow py-S-SO_3^{+} + e^{-} \xrightarrow{+H_2O} py-S-SO_4H + H^{+} \longrightarrow py-S-SO_4 + H^{+} + e^{-}} \\ \qquad \downarrow \qquad\qquad\qquad\qquad\qquad\qquad\qquad\qquad\qquad\qquad\qquad\qquad \downarrow \\ \mathrm{py + S_2O_3^{2-}} \qquad\qquad\qquad\qquad\qquad\qquad\qquad\qquad\qquad\qquad\qquad\qquad \mathrm{py-S + SO_4^{2-}} \end{array} \qquad (6\text{-}3)$$

Reactions (6-2) and (6-3) represent one possible pathway for the oxidation of the polysulphide. The key aspects are that: (i) oxidation occurs sequentially involving the addition of O from H_2O and the removal of electrons, (ii) the reaction occurs on anodic sites, independent of the cathodic process or the involvement of the oxidant, and (iii) a range of possible surface and dissolved intermediate species are possible (Borda et al. 2003, 2004).

Druschel and Borda (2006) present a schematic of a range of possible pathways for the oxidative dissolution of pyrite (Figure 6-1). Pathways 1A and 1B in the figure are similar to those described above in which the Fe-S bond breaks to produce $S_2O_3^{2-}$ (which can then react further to produce SO_4^{2-}, Pathway 1A) or in which the S-S bond breaks to ultimately form sulphate, possibly through a sulphite SO_3^{2-} solution intermediate (Pathway 1B). Pathway 2 is interesting in the current discussion because it involves congruent dissolution of the polysulphide, which is then postulated to be oxidised in solution. Finally, Pathway 3 involves photochemical processes.

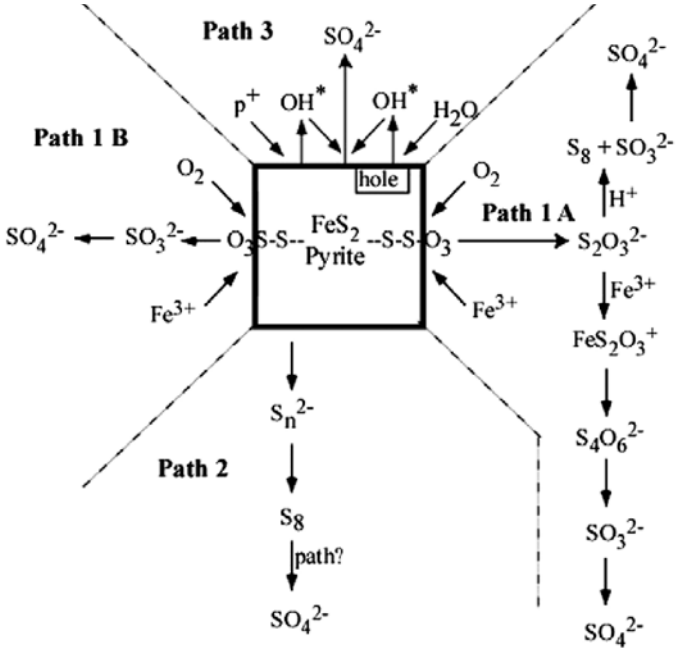

Figure 6-1. *Schematic of different pathways for the oxidative dissolution of pyrite (Druschel and Borda 2006). See text for explanation of different pathways.*

The cathodic reaction involves the overall reduction of Fe(III) or O_2 (or of other oxidants, discussed below). In the case of the oxidative dissolution of pyrite in O_2– or Fe^{3+}-containing solution, the actual oxidant is believed to be Fe^{3+}, either present in solution or formed by the homogeneous oxidation of Fe(II) by O_2. The cathodic reaction is believed to occur at Fe(II) sites on the pyrite surface (Rimstidt and Vaughan 2003). Electron transfer may be facilitated by shuttling of the Fe(II) site between Fe(II) and Fe(III) states. Although the cathodic reaction involves the transfer of fewer electrons and involves fewer steps, it is believed to be rate controlling.

A common observation is that the dissolved $[S_{TOT}]$:$[Fe_{TOT}]$ is < 2, even in acid solution in which the extent of precipitation of alteration products would be expected to be minimal (Descostes et al. 2004, 2010). This lead Descostes et al. (2004) to propose an alternative mechanism that includes the precipitation of elemental S

$$FeS_{2p} + 2.9O_2 + 0.6H_2O \rightarrow Fe^{2+} + 0.4S^0(s) + 1.6SO_4^{2-} + 1.2H^+ \quad (6\text{-}4)$$

where the stoichiometry was based on the observed $[S_{TOT}]$:$[Fe_{TOT}]$ of 1.6. Alternatively, Fe^{2+} sorption on the pyrite surface is also possible (Descostes et al. 2010).

Williamson and Rimstidt (1994) reviewed data from various kinetic studies of the rate of oxidative dissolution of pyrite by O_2 and by Fe^{3+} (under oxic and anoxic conditions). The best-fit rate law for O_2 is

$$\text{Rate}(\text{mol}\,\text{m}^{-2}\,\text{s}^{-1}) = 10^{-8.19(\pm 0.10)} \frac{m_{O_2}^{0.5(\pm 0.04)}}{m_{H^+}^{0.11(\pm 0.01)}} \quad (6\text{-}5)$$

where m is the molality in mol kg^{-1}. This expression is valid over the pH range 2–10 and for dissolved oxygen concentrations of $7 \cdot 10^{-7}$ to $2 \cdot 10^{-2}$ mol·dm^{-3} (0.02 to 620 mg/L). The corresponding rate expressions for oxidation by Fe^{3+} are

$$\text{Rate}(\text{mol}\,\text{m}^{-2}\,\text{s}^{-1}) = 10^{-8.58(\pm 0.15)} \frac{m_{Fe^{3+}}^{0.30(\pm 0.02)}}{m_{Fe^{2+}}^{0.47(\pm 0.03)} m_{H^+}^{0.32(\pm 0.04)}} \quad (6\text{-}6)$$

under anoxic conditions and

$$\text{Rate}(\text{mol}\,\text{m}^{-2}\,\text{s}^{-1}) = 10^{-6.07(\pm 0.57)} \frac{m_{Fe^{3+}}^{0.93(\pm 0.07)}}{m_{Fe^{2+}}^{0.40(\pm 0.06)}} \quad (6\text{-}7)$$

in the presence of O_2. The fractional reaction order with respect to the dissolved O_2 concentration in Equation (6-5) is consistent with an electrochemical mechanism.

A detailed discussion of the mechanism of the oxidative dissolution of pyrite is outside of the scope of the current review. In addition to the extensive literature on the dissolution behaviour in abiotic acidic environments, the effect of a number of other parameters have been considered:

- Oxidants other than O_2 or Fe^{3+}, including UV (Borda et al. 2003, 2004) and visible (Schoonen et al. 2000) light, H_2O_2/OH radicals (Schoonen et al. 2010), γ-radiation (Lefticariu et al. 2010), MnO_2 (Schippers and Jørgensen 2001, 2002), NO_3^- (Schippers and Jørgensen 2002), and amorphous precipitated Fe(III) (Schippers and Jørgensen 2002).
- Neutral and/or alkaline pH (Caldeira et al. 2003, 2010, Moses et al. 1987, Moses and Herman 1991, Todd et al. 2003, Williamson and Rimstidt 1994).
- Microbial effects (Bosch and Meckenstock 2012, Bosch et al. 2012, Brunner et al. 2008, Gleisner et al. 2006, Jørgensen et al. 2009, Lizama and Suzuki 1989, Rawlings et al. 1999, Schippers and Jørgensen 2001, 2002, Taylor et al. 1984, Torrentó et al. 2010).
- Temperature (Schoonen et al. 2000).
- Carbonate/bicarbonate (Caldeira et al. 2003, 2010, Ciminelli and Osseo-Asare 1995, Descostes et al. 2002, Huminicki and Rimstidt 2009, Nicholson et al. 1988, 1990).
- Ionic strength and Cl^- and SO_4^{2-} concentration (Williamson and Rimstidt 1994).
- Unsaturated or atmospheric environments (Jerz and Rimstidt 2004, Todd et al. 2003).

For the current report, it is important to note that the oxidative dissolution of pyrite can occur under anoxic conditions (sometimes, confusingly, referred to by some authors as dissolution under "anaerobic" conditions). The oxidative dissolution of FeS_{2p} by Fe^{3+} does occur under anoxic conditions, but is typically only sustained if O_2 is present to homogeneously oxidise Fe^{2+} to Fe^{3+}. Ultraviolet and visible light increases the rate of oxidative dissolution in the presence of Fe^{3+} or O_2 (Borda et al. 2003, 2004, Schoonen et al. 2000), although there is no evidence that either would sustain dissolution in the absence of the other oxidants in the system. On the other hand, γ-irradiation alone will cause oxidative dissolution by the reaction of OH radicals, although Fe^{3+} species are inevitably produced in solution because of the irradiation (Lefticariu et al. 2010). Schippers and Jørgensen (2001, 2002) studied the effect of MnO_2, NO_3^-, and precipitated amorphous Fe(III) oxide on the oxidative dissolution of pyrite in anoxic marine sediments containing natural microbial populations. Manganese dioxide was found to oxidise FeS_{2p} under both biotic and abiotic conditions. However, neither NO_3^- nor amorphous Fe(III) oxide acted as oxidants for pyrite under biotic or abiotic conditions, although both species did oxidise iron sulphide (FeS) in the presence of microbes, clearly showing the greater stability of pyrite compared with FeS.

The pH of pore water in the buffer and backfill materials in the repository is expected to be slightly alkaline because of buffering by calcite mineral impurities. As such, the dissolution behaviour of pyrite at neutral or moderately alkaline pH is of more interest than that at low pH designed to simulate acid rock drainage conditions. Despite its lower solubility, there is evidence that Fe^{3+} still acts an the oxidant in neutral and alkaline solution, although O_2 is required to sustain the reaction (Moses and Herman 1991, Moses et al. 1987). Precipitation of alteration products on the pyrite surface is also an issue in neutral and alkaline solution (Caldeira et al. 2003, 2010, Huminicki and Rimstidt 2009, Todd et al. 2003). The alteration products tend to be ferric species, including precipitated $Fe_2(SO_4)_3$ and $FeOH(SO_4)$, with FeOOH or $Fe(OH)_3$ reported with increasing pH. These species tend to result in a decrease in dissolution rate with time because the precipitated film restricts O_2 transport to the pyrite surface (Huminicki and Rimstidt 2009).

Microbes are known to accelerate the dissolution of pyrite in acidic solutions by a factor of up to 10^6 (Vaughan 2005). Species such as *Thiobacillus ferrooxidans* facilitate the oxidation of both Fe^{2+} and sulphur. Gleisner et al. (2006) report an indirect effect of microbial activity through the oxidation of Fe^{2+} to Fe^{3+}, but report no enhancement in the rate. As noted above, Schippers and Jørgensen (2001, 2002) found that naturally occurring microbes in anoxic sea sediments did not catalyse the oxidation of pyrite by NO_3^- or amorphous Fe(III) oxide. However, recently the oxidation of pyrite supported by the microbial reduction of nitrate has been reported (Bosch and Meckenstock 2012, Bosch et al. 2012, Jørgensen et al. 2009, Torrentó et al. 2010).

Jerz and Rimstidt (2004) studied the oxidation of pyrite in humid air. At a constant relative humidity (RH) of 96.7%, the dissolution rate was found to decrease with time, which was attributed to increasing transport control by O_2 diffusion across a thickening aqueous film containing $FeSO_4$ and H_2SO_4. Because the RH was controlled, the solution layer thickened as dissolution proceeded as the solution composition is constant at a given RH. At RH values less than 95%, a precipitated ferrous sulphate film formed, presumably because this value is below the deliquescence RH for iron sulphate. Preferential precipitation at grain boundaries caused the pyrite crystals to disaggregate.

6.2 Reductive dissolution

The reductive dissolution of pyrite is of interest because it would not only release sulphide but also result in the formation of a form of iron sulphide more soluble than pyrite, such as pyrrhotite or troilite.

Reduction of pyrite is known to occur at elevated temperatures in H_2 atmospheres (Lambert et al. 1980, 1998). In inert atmospheres, pyrite is reduced at high temperatures to pyrrhotite along with the formation of elemental sulphur. In the presence of H_2, both pyrrhotite and H_2S are formed, the overall reaction being (Hol et al. 2010, Lambert et al. 1998)

$$FeS_{2p} + (1–x)H_2 \rightarrow FeS_{1+x} + (1–x)H_2S \quad (6\text{-}8)$$

However, the kinetics of the reaction are not significant at temperatures below 300–400°C and the process exhibits a strong temperature dependence with an activation energy of 90 kJ/mol (Lambert

et al. 1998). Hol et al. (2010) tried to induce the reduction of pyrite at more moderate temperatures (35°C and 55°C) and H_2 pressures (0.11–0.14 MPa) using bacterial communities, including sulphate reducers. Despite suppressing unwanted microbial reduction processes, such as methane formation and sulphate reduction, no reduction of pyrite was observed.

As part of the study of the impact of repository conditions on the pyrite contained in Callovo-Oxfordian clay in the French nuclear waste management programme, Truche et al. (2010) have demonstrated the reductive dissolution of pyrite with H_2 at temperatures between 90 and 180°C. Experiments were performed in a dilute NaCl solution (0.027 mol·dm^{-3}) at pH 6.9–8.7 and buffered by crushed calcite. Reduction of FeS_{2p} to FeS_{1+x} ($0 < x < 0.125$) was demonstrated for H_2 partial pressures of 0.8 MPa and 1.8 MPa. Figure 6-2 shows the results of selected experiments at temperatures of 90°C and 150°C, for H_2 partial pressures of 0 MPa and 0.8 MPa, and for different sizes of pyrite particles (with correspondingly different reactivity). Dissolved HS^- is observed at both 90°C and 150°C with 0.8 MPa H_2 for the finer (and more reactive) pyrite particle size. Although no HS^- was observed for the coarser-grained material at 90°C, sulphide was observed in other experiments with this material at higher temperature and/or H_2 pressure. The [HS^-] appears to reach a constant value, possibly reflecting an equilibrium solubility. The increase in dissolution rate with temperature is equivalent to an activation energy of 53 kJ/mol. No HS^- is observed at 150°C in the absence of H_2, even with the finer-grained material.

Truche et al. (2010) developed an expression for the release of HS^- (N in mol m^{-2}) as a function of time (t in hours), H_2 pressure (p_{H_2} in Pa) and temperature (T in K)

$$\log N = -5.22 + 0.47 \log t + 1.10 \log p_{H_2} - \frac{2755}{T} \qquad (6\text{-}9)$$

The pyrrhotite formed by the reduction process forms a crust over the pyrite core, with the rate jointly controlled by the pyrite reduction process and the diffusion of HS^- through the surface film. Betelu et al. (2012) have shown that the rate of reductive dissolution in the presence of H_2 can be increased by cathodic polarisation.

Hydrogen is not the only reductant that may lead to the reductive dissolution of pyrite. Luther (1987) has shown that the experimentally reported reduction of FeS_{2p} by Cr(II) is consistent with molecular orbital theory considerations.

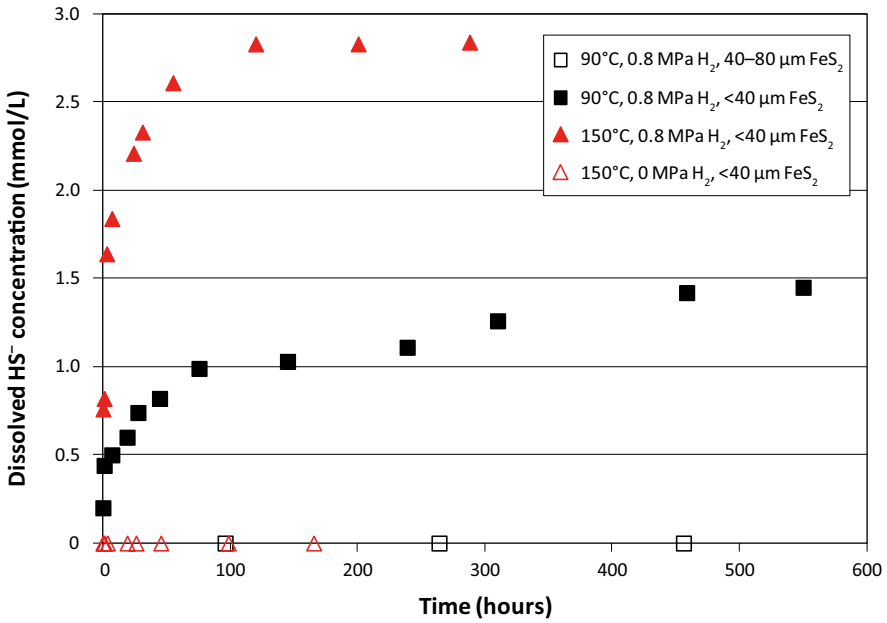

Figure 6-2. *Time dependence of the dissolved sulphide concentration as the result of the reductive dissolution of pyrite by hydrogen. Based on data by Truche et al. (2010).*

6.3 Chemical dissolution

Very few studies of the chemical dissolution of FeS_{2p} have been published. Although Druschel and Borda (2006) speculate on a polysulphide oxidative dissolution pathway that essentially involves a chemical dissolution process followed by homogeneous oxidation of the dissolved polysulphide (Pathway 2, Figure 6-1), these authors provide no direct evidence in support of such a mechanism. The indirect evidence suggested for such a pathway includes the observation of elemental sulphur reported by a number of authors and solution $[SO_4^{2-}]$:[Fe] ratios less than two, the latter evidence implying that not all of the dissolved polysulphide is subsequently fully oxidised to sulphate.

Weerasooriya and Tobschall (2005) report dissolution of pyrite in anaerobic solutions. Dissolved iron was measured in acidified 0.1 mol·dm^{-3} $NaClO_4$ solutions at pH < 4.5, which was ascribed to a surface complexation process that resulted in the release of Fe^{2+}. The authors report both H_2S in acidic solution and S_2^{2-} in alkaline solution (>pH 10), although there is no description of how the latter was measured. The detection of sulphide in solution was taken as an indication of pyrite dissolution. However, the exact experimental details are not clear, since the authors refer to the effect of O_2 in the text and it is not clear whether the data shown were measured under anaerobic conditions as implied in the Abstract. No dissolution rates were given and equilibration times were limited to 30 minutes.

Thomas et al. (2001) report pyrite dissolution rates in argon-purged 0.1 mol·dm^{-3} perchloric acid (pH 1) solution. A peak Fe release (dissolution) rate of $6 \cdot 10^{-9}$ mol m^{-2} s^{-1} (0.2 mol m^{-2} y^{-1}) was reported after 4 h exposure, which then decreased to zero by the end of the 28-h-duration experiment.

6.4 Electrochemistry of pyrite

There is an extensive literature on electrochemical measurements on pyrite. However, the majority of studies have focussed on the oxidation of pyrite, primarily in acidic solution, and are not discussed in detail here. Among the studies that have been performed are the following:

- Mechanism and electrochemical kinetics (Biegler and Swift 1979, Hamilton and Woods 1981, Holmes and Crundwell 2000, Kelsall et al. 1999, Liu et al. 2008, 2009, Mycroft et al. 1990).
- Semi-conductivity, impurity content, and reactivity (Biegler 1976, Cruz et al. 2001, Kelsall et al. 1999, Lehner et al. 2007).
- Film growth and characterisation (Giannetti et al. 2006, Mycroft et al. 1990).
- The oxygen reduction reaction (Ahlberg and Broo 1996, Biegler 1976, Rand 1977).
- Measurement of the open-circuit potential (Moslemi et al. 2011).
- The effect of microbes on pyrite oxidation (Cabral and Ignatiadis 2001, Holmes et al. 1999).

The electrochemical reduction of pyrite has been proposed as a method for desulphurising coal (Zhao et al. 2005, 2008). Tao et al. (1994, 2003) have studied the electrochemical behaviour of freshly fractured pyrite in deaerated borate buffer solution at pH 9.2. Figure 6-3 shows a cyclic voltammogram of pyrite from a Chinese coal sample measured in deaerated pH 9.2 borate buffer solution at room temperature. The authors identified three anodic peaks (labelled I, II, and III) and three cathodic peaks (labelled IV, V, and VI) on the voltammogram. Tao et al. (2003) assigned these peaks to the following processes:

I $\quad Fe + 2OH^- \rightarrow Fe(OH)_2 + 2e^-$ (6-10)

II $\quad$ initial oxidation of FeS_{2p} (6-11)

III $\quad FeS_{2p} + 11H_2O \rightarrow Fe(OH)_3 + 2SO_4^{2-} + 19H^+ + 15e^-$ (6-12)

IV $\quad (n–1)Fe(OH)_3 + FeS_n + 3(n–1)e^- \rightarrow nFeS + 3(n–1)OH^-$ (6-13)

V $\quad S^0 + H^+ + 2e^- \rightarrow HS^-$ (6-14)

VI $\quad FeS_{2p} + H_2O + 2e^- \rightarrow FeS + HS^- + OH^-$ (6-15a)

$\quad FeS_{2p} + 2H_2O + 4e^- \rightarrow Fe + 2HS^- + 2OH^-$ (6-15b)

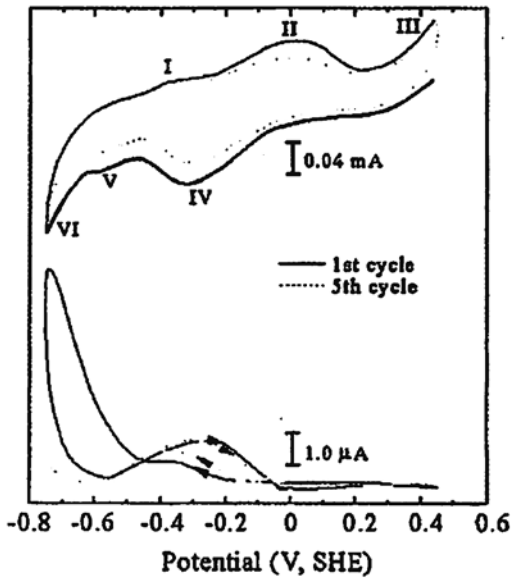

Figure 6-3. *Cyclic voltammetric behaviour of a pyrite rotating disc electrode in borate buffer at pH 9.2 and the corresponding current for a gold ring at a potential of +0.25 V_{SHE} (Tao et al. 2003). Although the authors suggest both 1st and 5th cycles are shown, the curves for the latter are not visible on the original. Electrode rotation rate 2,000 rpm, potential scan rate not defined.*

where the Fe oxidised in Reaction (6-10) and the sulphur reduced in Reaction (6-14) were formed during the preceding cathodic and anodic scans, respectively. Cathodic feature VI is accompanied by a large ring oxidation current, which Tao et al. (2003) attributed to the oxidation of HS^- to S^0.

The assignment of these peaks is based on earlier studies by Ahlberg et al. (1990) and Hamilton and Woods (1981). However, little supporting evidence is provided in these studies for the assignment of the different peaks and, indeed, Hamilton and Woods (1981) reported fewer voltammetric features and Ahlberg et al. (1990) report a greater number of anodic and cathodic peaks than observed by Tao et al. (2003). Therefore, the assignment of the different peaks is somewhat uncertain and, in particular, that for the reduction of FeS_{2p} (peak VI in Figure 6-3), which Ahlberg et al. (1990) report as beginning at approximately –0.8 V_{SCE} at pH 11. Ahlberg et al. (1990) did not have the advantage of using a rotating ring-disc electrode, but one must wonder whether the corresponding ring oxidation current observed by Tao et al. (2003) may not be the result of the oxidation of H_2 produced by the reduction of H_2O on the disc electrode at potentials more-negative than –0.65 V_{SHE} (the reversible potential for the evolution of H_2 is approximately –0.54 V_{SHE} at pH 9.2). Nevertheless, the potential of –0.65 V_{SHE} for the onset of measurable pyrite reduction is consistent with the equilibrium potential for Reaction (6-15a). Using the free energy of formation value for FeS_{2p} and HS^- in Table 5-1 and corresponding values for pyrrhotite and troilite of –98.9 kJ/mol and –102.9 kJ/mol, respectively (Robie and Hemingway 1995), the standard potential E^0 for Reaction (6-15a) is –0.794 V_{SHE} and –0.774 V_{SHE} for pyrite reduction to pyrrhotite and troilite, respectively. At pH 9.2, the equilibrium potentials for this reaction are –0.475 V_{SHE} and –0.455 V_{SHE} for pyrrhotite and troilite, respectively. Thus, in electrochemical terms, compared with the potential of –0.65 V_{SHE} at which Tao et al. (2003) report a measurable pyrite reduction current, the process exhibits an overpotential 175–200 mV.

Tao et al. (1994, 2003) report the "stable" potential of freshly fractured pyrite to be –0.28 V_{SHE} in deaerated borate buffer at pH 9.2. This potential was the value at which freshly fractured pyrite surfaces exhibited no net current (i.e., neither oxidation nor reduction) and which, therefore, is a measure of what is more commonly referred to as the open-circuit or corrosion potential (E_{CORR}). If we take this value as representative of E_{CORR} of pyrite under anaerobic conditions, then the data in Figure 6-3 suggests that we need to polarise the surface by approximately –0.4 V in order to cathodically reduce FeS_{2p} to FeS via Reaction (6-15a), if we assume that peak VI corresponds to the reduction of pyrite. Thus, in order to reductively dissolve pyrite under freely corroding conditions (as might occur in the repository), the presence of a reducing species with a sufficiently negative equilibrium potential to cathodically polarise the potential of the pyrite by 0.4 V to –0.65 V_{SHE} is required.

By way of example, let us assume that H_2 is the reductant and that the reduction of pyrite is accompanied by the oxidation of hydrogen

$$H_2 \rightarrow 2H^+ + 2e^- \quad (6\text{-}16)$$

which is essentially the process occurring in the work of Truche et al. (2010), since it is believed to follow an electrochemical mechanism (Betelu et al. 2012). The H_2 pressure required to produce an equilibrium potential of –0.65 V_{SHE} at pH 9.2 and 25°C is estimated to be 350 MPa. Truche et al. (2010) did not perform experiments at temperatures below 90°C, but the estimated H_2 pressure is not inconsistent with their findings.

7 Implications for repository performance

Various aspects of the properties of pyrite are important for the performance of the repository system, including:

- The initial state of the pyrite in the bentonite.
- The evolution of the pyrite behaviour in the buffer and backfill, especially the release of sulphide species and the extent of oxidative, reductive, and chemical dissolution.
- The consequences for corrosion of the canister, especially the (beneficial) consumption of O_2 and the (detrimental) formation of dissolved sulphur species that might support corrosion during the anoxic period.

7.1 Initial state of pyrite in bentonite

There is no information on the initial state of the pyrite impurities in the bentonite clay, other than the likely range of the pyrite content. If we assume that the pyrite was formed by a low-temperature dissolution-precipitation mechanism, as in the case of the pyrite inclusions in the bentonite sample from Zao, Japan (Fukushi et al. 2010), then the pyrite is more likely to exhibit p-type semi-conducting properties than n-type, based on the evidence summarised in Section 2.1.3.

During exposure to the atmosphere during mining and milling operations, the pyrite could undergo oxidative dissolution if moisture is present, although the existence of pyrite in the processed clay suggests that the extent of such processes are limited. Since, the system is highly pH-buffered (because of the presence of calcite), the pyrite surface is likely to become encrusted with alteration products (Section 6.1). If oxidation occurs under unsaturated (atmospheric) conditions, the precipitated phase may be $FeSO_4$ (Jerz and Rimstidt 2004). If oxidation occurs under saturated conditions, then the alteration products are more likely to include ferric species, such as $Fe_2(SO_4)_3$ and $FeOH(SO_4)$, with FeOOH or $Fe(OH)_3$ possible with increasing pH (Caldeira et al. 2003, 2010, Huminicki and Rimstidt 2009, Todd et al. 2003).

However, because of the lack of direct characterisation of the pyrite particles in bentonite clays, this suggested initial state of the pyrite should be treated cautiously.

7.2 Evolution of pyrite behaviour in repository

7.2.1 In the buffer

Pyrite in the buffer material will be exposed first to warm, oxic conditions and then, as the repository environment evolves, an indefinite cool, anoxic period. Because microbial activity is suppressed virtually completely in highly compacted bentonite, pyrite will only react abiotically in the buffer.

During the oxic phase, the pyrite will undergo similar processes to those described above during the mining and milling operations. During the post-closure period, however, the temperature will be higher and, depending upon the permeability of the host rock, the buffer may be saturated. These reactions will consume a fraction of the initially trapped atmospheric O_2, resulting in the formation of sulphate and the dissolution of calcite in response to the generation of H^+. The pyrite particles will become further encrusted with a layer of alteration products, most likely ferric species. The presence and further growth of this outer layer will reduce the rate of oxidation over that observed under acidic, film-free conditions.

In terms of the release of sulphur species during the oxic period, the predominant species will be sulphate. Depending upon the pathway for pyrite oxidation (Figure 6-1), small amounts of other sulphur oxyanions may be released into solution, such as thiosulphate $S_2O_3^{2-}$, polythionates $S_nO_6^{2-}$, and sulphite SO_3^{2-} (Chandra and Gerson 2010, Moses et al. 1987). However, if O_2 is still present in the buffer pore water, then these species may be homogeneously oxidised further.

Once anoxic conditions become established, the pyrite is likely to react very slowly, if at all. In the absence of microbial activity or a high pressure of H_2, the pyrite will be neither further oxidised nor undergo reductive dissolution.

Truche et al. (2010) have shown that pyrite can be reduced to pyrrhotite by H_2 at elevated temperatures, accompanied by the release of sulphide. However, there is no evidence that this reaction occurs at any significant rate at the lower temperatures expected during the anoxic period. Furthermore, there will be limited amounts of H_2 produced in the buffer material. Corrosion of copper by HS^-, with the accompanying formation of H_2, will only result from the diffusion of HS^- from the backfill or groundwater. The rate of this process is estimated to be equivalent to a corrosion rate of < 1 nm/y (King et al. 2011a, b), and at this rate the H_2 produced will diffuse away from the canister as dissolved H_2 and will not accumulate as a H_2 gas phase of elevated pressure (King 2012).

Despite the fact that reductive dissolution of FeS_{2p} by H_2 is unlikely to occur in the buffer, it is interesting to apply the sulphide production rate expression (Equation (6-9)) developed by Truche et al. (2010) to the "what-if" scenario considered by SKB (2010a). In this scenario, it was assumed that the copper is corroded by water as proposed by Szakálos et al. (2007) and that an equilibrium H_2 partial pressure of 0.001 bar is attained. Let us further assume that Equation (6-9) is valid at this H_2 partial pressure and at a temperature of 80°C (the maximum canister temperature), although these conditions fall outside those investigated by Truche et al. (2010). We can then use Equation (6-9) to predict the quantity of HS^- produced by the reductive dissolution of pyrite by H_2 as a function of time.

Figure 7-1 shows the predicted amount of HS^- produced by the reductive dissolution of pyrite expressed in terms of moles per m^2 pyrite surface and per borehole.[1] The rate of sulphide production is low and even after 1 million years amounts to only 0.008 mol per borehole. For the reaction

$$2Cu + HS^- + H_2O \rightarrow Cu_2S + H_2 + OH^- \quad (7\text{-}1)$$

the predicted depth of corrosion due to this source of sulphide is 6 nm.

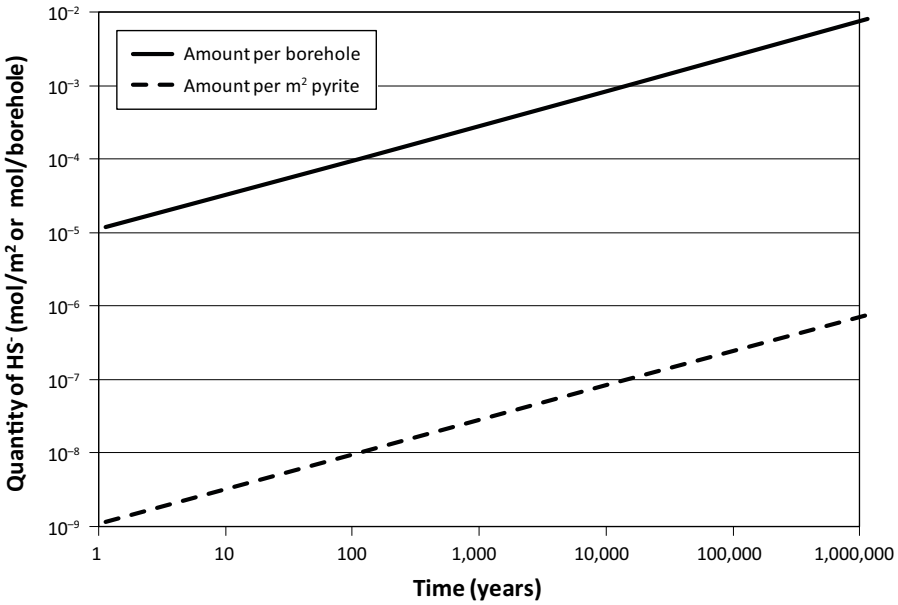

Figure 7-1. *Estimated production of sulphide by the reductive dissolution of pyrite by hydrogen for a H_2 pressure of 0.001 bar and a temperature of 80°C (based on data of Truche et al. 2010).*

[1] For this calculation, it was assumed that the pyrite exists as spherical particles of radius 10 µm and, hence, a surface area:volume ratio of $3 \cdot 10^4$ cm^{-1}. It was further assumed that the MX-80 bentonite contains 0.07 wt.% FeS_{2p} (SKB 2010a), that the canister has a length of 4.835 m and a radius of 0.525 m (SKB 2010a), the borehole is 6.68 m deep and 1.77 m diameter (SKB 2010b), and is filled with compacted bentonite with an average dry density of 1,600 kg m^{-3} (SKB 2011). The density of pyrite was taken to be 5 g cm^{-3} (CRC 1982). Based on these values, the borehole is estimated to contain 23,000 kg bentonite containing 16 kg pyrite or 133 mol with a volume of 3,200 cm^3. The surface area of this pyrite is 10^4 m^2 per borehole.

In the absence of oxidative or reductive dissolution, the pyrite, or more-accurately, the Fe(III)-encrusted pyrite particles will be subject to chemical dissolution only. At the expected pore-water pH of 7–8 both Fe(III) and the pyrite itself have very low solubility. In the case of pyrite, the solubility (expressed in terms of the HS^- or HS_2^- concentration) is of the order of 10^{-11}–10^{-12} mol·dm^{-3} (Figure 5-4). The dissolution rate will be determined by the rate at which the dissolved sulphide or polysulphide can diffuse away from the pyrite particle.

7.2.2 In the backfill

The behaviour of pyrite in the backfill will be similar to that in the buffer material, except that there is the possibility of microbially-mediated dissolution processes.

Under oxic conditions, therefore, the oxidative dissolution of pyrite may be enhanced by the action of *Thiobacillus ferrooxdians* or similar microbes (Gleisner et al. 2006, Vaughan 2005). Microbial enhancement will increase the rate at which O_2 is consumed but will not change the mechanism, since the role of *T. ferrooxidans* is to promote the oxidation of Fe^{2+} to Fe^{3+} rather than to fundamentally change the mechanism. Thus, as in the buffer, oxidative dissolution will largely be accompanied by the formation of sulphate, with the formation of limited amounts of other sulphur oxyanions possible, depending upon the pathway for pyrite oxidation.

During the long-term anoxic period, further oxidation of the pyrite is possible if suitable electron acceptors and microbes are present. Nitrate reduction, promoted by species such as *T. denitrificans* (Bosch et al. 2012), has been shown to support the oxidation of pyrite (Bosch and Meckenstock 2012, Bosch et al. 2012, Jørgensen et al. 2009, Torrentó et al. 2010), but there is no apparent source of nitrate in the backfill. It is interesting to note that, despite attempts, the microbially mediated reduction of amorphous precipitated Fe(III), as might be present in the crust of alteration products on the partially oxidised pyrite particles, has not be shown to similarly support pyrite oxidation (Schippers and Jørgensen 2001, 2002).

It is significant that, although microbial activity has been shown to promote the oxidation of pyrite under anoxic conditions, there is no evidence that anaerobes can promote the reductive dissolution of pyrite (Hol et al. 2010).

Reductive dissolution promoted by H_2 is theoretically possible in the backfill during the anoxic period but, as in the case of the buffer, there is no obvious source of H_2 in the repository (other than the anaerobic corrosion of any rock bolts) and the temperatures in the backfill will be significantly lower than those at which Truche et al. (2010) observed pyrite reduction. Furthermore, since microbial activity is possible in the backfill, any H_2 that does form will likely be rapidly consumed by sulphate-reducing bacteria (King et al. 2010).

Thus, as for the buffer material, the most likely dissolution mechanism of the pyrite in the backfill during the long-term anaerobic period is slow chemical dissolution.

7.3 Consequences for corrosion of the canister

Pyrite can influence the corrosion behaviour of the canister at all stages in the evolution of the repository environment. During the oxic phase, pyrite will undergo oxidative dissolution resulting in the consumption of O_2, the latter then not being available to support the corrosion of the canister. The predominant oxidation product will be sulphate SO_4^{2-} which, in the absence of microbial activity, is inert. In addition, however, small amounts of other sulphur oxyanions, such as thiosulphate $S_2O_3^{2-}$ and tetrathionate $S_4O_6^{2-}$, and polysulphides S_n^{2-} may be produced. Macdonald and Sharifi-Asl (2011) have reported an extensive thermodynamic analysis of possible reactions between Cu and a large number of sulphur species. Table 7-1 summarises a number of the reactions considered and indicates whether the particular sulphur species was found to "activate" copper or not, a term used by Macdonald and Sharifi-Asl (2011) to indicate if corrosion was possible. In general, sulphide species, polysulphides, polythionates ($S_xO_6^{2-}$) and thiosulphate were found to "activate" corrosion, whereas polythiosulphates ($S_xO_3^{2-}$, x = 3–6) were found not to.

When considering the net effect of these reactions on the corrosion of the canister, we must remember that oxidant, in the form of the initially trapped atmospheric O_2, is consumed in producing these sulphur species. Thus, when carrying out a mass-balance calculation to determine how much corrosion occurs, we must be careful not to double-count the available electron acceptors. For example, thiosulphate can oxidise copper according to

$$2Cu + S_2O_3^{2-} = Cu_2S + SO_3^{2-} \quad (7\text{-}2)$$

However, O_2 is consumed in the formation of the $S_2O_3^{2-}$ via the oxidation of pyrite

$$FeS_{2p} + 1.5O_2 \rightarrow S_2O_3^{2-} + Fe^{2+} \quad (7\text{-}3)$$

where Reaction (7-3) represents the overall stoichiometry of the process but not necessarily the detailed mechanism, which involves the interaction of H_2O with polysulphide groups at anodic sites on the pyrite surface.

The net effect of Reactions (7-2) and (7-3), however, is that 1.5 mol O_2 results in the corrosion of only 2 mol Cu, whereas the oxidation reaction

$$6Cu + 1.5O_2 \rightarrow 3Cu_2O \quad (7\text{-}4)$$

would result in the consumption of three times as much copper. Thus, even though some of the intermediate sulphur oxyanions may themselves cause corrosion of the copper, there is still a net consumption of the available oxidant as a result of the oxidative dissolution of pyrite.

In some cases, however, the sulphur species can promote corrosion with the evolution of H_2 from the reduction of H_2O. For example, consider the polysulphide species S_4^{2-} which reacts with copper as follows (Table 7-1)

$$8Cu + S_4^{2-} + 2H^+ = 4Cu_2S + H_2(g) \quad (7\text{-}5)$$

The precise mechanism by which the polysulphide species might form is uncertain, but it involves the oxidation of sulphur in pyrite from a mean oxidation state of –1 to a mean oxidation state of –0.5 in S_4^{2-}. If we assume the oxidant is O_2, then 0.5 mol O_2 will produce 1 mol S_4^{2-}. This polysulphide can then react with 8 mol Cu (Reaction (7-5)), four times more than the equivalent 0.5 mol O_2 would via Reaction (7-4).

A detailed analysis of all of the reactions investigated by Macdonald and Sharifi-Asl (2011) and a proper accounting for the electron-balance is beyond the scope of the current report. However, it is likely that only small amounts of these "activating" sulphur species will be produced during the oxidative dissolution of pyrite and that the major product will be the (kinetically) inert sulphate ion.

Under anaerobic conditions, all three forms of dissolution (oxidative, reductive, and chemical) are theoretically possible, although are unlikely to occur to a significant extent. Continued oxidative dissolution is possible in the backfill if there is a suitable source of electron acceptors (e.g., NO_3^-) and if the other requirements for sustained microbial activity are met. However, there is no obvious source of large amounts of NO_3^- in the backfill and any H_2 that might be present will likely be consumed by sulphate-reducing bacteria.

Reductive dissolution by H_2 seems unlikely to occur in either the buffer or backfill as there is no source of the high H_2 pressures required to sustain significant pyrite reduction.

Therefore, the only viable mechanism for the release of sulphide or polysulphide during the long-term anaerobic phase is chemical dissolution. The extent of dissolution will be limited, however, by the low solubility of pyrite and the slow transport of dissolved HS^- or HS_2^- from the pyrite to the canister.

In summary, the pyrite in the buffer and backfill is unlikely to be a significant source of reactants for the copper canister. The amount of potentially aggressive dissolved oxidation products is expected to be small and the availability of sulphide and HS_2^- to support corrosion under anaerobic conditions will be limited by the extremely low solubility of FeS_{2p} and the restrictive mass-transport conditions in the bentonite. Thus, pyrite will only adversely impact the corrosion behaviour of the canister if the small amounts of sulphur species promote highly localised forms of corrosion.

Table 7-1. Selection of reactions between copper and various sulphur species studied by Macdonald and Sharifi-Asl (2011).

Reaction	Does the reactant act as an "activator"?*
$2Cu + H_2S_2O_3 = Cu_2S + SO_3^{2-} + 2H^+$	Yes
$2Cu + H_2S_2O_4 = Cu_2S + SO_4^{2-} + 2H^+$	Yes
$2Cu + HS_2O_3^- = Cu_2S + SO_3^{2-} + H^+$	Yes
$2Cu + HS_2O_4^- = Cu_2S + SO_4^{2-} + H^+$	Yes
$2Cu + S^{2-} + 2H^+ = Cu_2S + H_2(g)$	Yes
$2Cu + H_2S = Cu_2S + H_2(g)$	Yes
$2Cu + S_2O_3^{2-} = Cu_2S + SO_3^{2-}$	Yes
$2Cu + S_2O_4^{2-} = Cu_2S + SO_4^{2-}$	Yes
$4Cu + S_2^{2-} + 2H^+ = 2Cu_2S + H_2(g)$	Yes
$4Cu + S_3O_3^{2-} = 2Cu_2S + SO_3^{2-}$	No
$4Cu + S_4O_6^{2-} = 2Cu_2S + SO_3^{2-} + SO_3(aq)$	Yes
$6Cu + S_3^{2-} + 2H^+ = 3Cu_2S + H_2(g)$	Yes
$6Cu + S_4O_3^{2-} = 3Cu_2S + SO_3^{2-}$	No
$6Cu + S_5O_6^{2-} = 3Cu_2S + SO_3^{2-} + SO_3(aq)$	Yes
$8Cu + S_4^{2-} + 2H^+ = 4Cu_2S + H_2(g)$	Yes
$8Cu + S_5O_3^{2-} = 4Cu_2S + SO_3^{2-}$	No
$8Cu + S_6O_6^{2-} = 4Cu_2S + SO_3^{2-} + SO_3(aq)$	Yes
$10Cu + S_5^{2-} + 2H^+ = 5Cu_2S + H_2(g)$	Yes
$10Cu + S_6O_3^{2-} = 5Cu_2S + SO_3^{2-}$	No
$10Cu + S_7O_6^{2-} = 5Cu_2S + SO_3^{2-} + SO_3(aq)$	Yes
$12Cu + S_6^{2-} + 2H^+ = 6Cu_2S + H_2(g)$	Yes
$12Cu + S_7O_3^{2-} = 6Cu_2S + SO_3^{2-}$	No
$4Cu + HS_3O_3^- = 2Cu_2S + SO_3^{2-} + H^+$	Yes

* A term used by Macdonald and Sharifi-Asl (2011) to indicate whether the sulphur species promotes corrosion of copper.

8 Summary and conclusions

A review has been conducted of the properties and behaviour of pyrite and of the implications for the corrosion of copper canisters in a KBS-3 type repository.

Pyrite (FeS_{2p}) is an Fe(II) polysulphide with a cubic structure and exhibits semi-conducting properties, determined primarily by the nature and extent of doping by cationic impurity elements. Pyrite is formed by either precipitation from high-temperature melts or by aqueous-based dissolution-precipitation processes at lower temperatures. Pyrite is the most thermodynamically stable of a number of different iron sulphides found in nature.

Bentonite clays typically contain pyrite as a minor constituent, with a content of less than approximately 1 wt.%. Some sources of bentonite, however, contain little or no pyrite. Little is known about the composition or properties of the pyrite in the bentonite clays proposed for use in the repository.

The speciation of sulphide and polysulphide in aqueous solution is well understood and the relative distribution of species as a function of pH is known.

The solubility of pyrite is so low that it cannot be experimentally measured. Instead, the concentration of dissolved species in equilibrium with the solid can be estimated based on estimates of the free energy of reaction of assumed dissolution processes. At pH 7–8, representative of that of bentonite pore water, the concentration of HS^- or HS_2^- in equilibrium with FeS_{2p} is of the order of 10^{-12}–10^{-11} mol·dm^{-3} at 25°C, approximately ten orders of magnitude lower than the corresponding concentration of HS^- in equilibrium with mackinawite FeS_m or greigite Fe_3S_{4g} at the same pH.

Pyrite can dissolve oxidatively, reductively, or chemically (congruently). These mechanisms are distinguished by the change in oxidation state of the sulphur, which either increases (from a mean value of –I in pyrite to as high as VI for the predominant dissolution product sulphate SO_4^{2-}), decreases (from –I to –II), or remains unchanged in the case of oxidative, reductive, and chemical dissolution, respectively. Upon dissolution, the oxidation state of the Fe remains unchanged at II (unless it is subsequently oxidised by O_2 under oxic conditions).

There is an extensive literature on the oxidative dissolution of FeS_{2p} because of the importance of this process in acid rock drainage and mineral extraction. The predominant product of the reaction is SO_4^{2-}, although smaller amounts of intermediate oxidation products such as sulphur, sulphite, thiosulphate, etc. are also reported.

There has been far less study of the reductive dissolution of pyrite, a process that not only leads to the release of sulphide but also produces less-stable (and, hence, more-soluble) iron sulphides such as pyrrhotite or troilite. The reduction of pyrite is well known in H_2 gas atmospheres at temperatures above 400°C, and there is also evidence for the reaction in aqueous solution at temperatures of 90–180°C with H_2 overpressures of 0.8 MPa and 1.8 MPa. There is no evidence for microbially enhanced pyrite reductive dissolution.

The chemical dissolution of pyrite has been demonstrated in acid solution, but no detailed study of the dissolution kinetics has been published.

In terms of the probable behaviour of pyrite in the repository, the predominant process will be the oxidative dissolution of FeS_{2p} during the early warm, aerobic period. This will result in the consumption of a portion of the initially trapped atmospheric O_2 and the formation of SO_4^{2-} and, possibly, smaller quantities of other sulphur and sulphur oxyanions species, some of which may support corrosion of the canister if they reach the copper surface.

During the long-term anaerobic phase, oxidation of pyrite in the backfill may continue if there is a suitable electron acceptor (such as nitrate NO_3^-) available and suitable conditions for microbial activity. Because of the use of highly compacted bentonite, there will be no microbial activity and no oxidative dissolution of pyrite in the buffer during the anaerobic period. It seems unlikely that either the temperature and/or H_2 pressure will be high enough in the repository to sustain the reductive dissolution of pyrite during this period. Therefore, only chemical dissolution of pyrite is likely in the long term, with the rate limited by the slow diffusion of HS^-/HS_2^- away from the dissolving surface.

In summary, therefore, the pyrite in the buffer and backfill material is likely to consume a fraction of the initially trapped atmospheric O_2 but is unlikely to produce a significant quantity of dissolved sulphur species that could support corrosion of the canister.

References

SKB's (Svensk Kärnbränslehantering AB) publications can be found at www.skb.se/publications.

Abraitis P K, Pattrick R A D, Vaughan D J, 2004. Variations in the compositional, textural and electrical properties of natural pyrite: a review. International Journal of Mineral Processing 74, 41–59.

Ahlberg E, Broo A E, 1996. Oxygen reduction at sulphide minerals. 3. The effect of surface pre-treatment on the oxygen reduction at pyrite. International Journal of Mineral Processing 47, 49–60.

Ahlberg E, Forssberg K S E, Wang X, 1990. The surface oxidation of pyrite in alkaline solution. Journal of Applied Electrochemistry 20, 1033–1039.

Arcos D, Grandia F, Domènech C, Fernández A M, Villar M V, Muurinen A, Carlsson T, Sellin P, Hernán P, 2008. Long-term geochemical evolution of the near field repository: insights from reactive transport modelling and experimental evidences. Journal of Contaminant Hydrology 102, 196–209.

Benning L G, Wilkin R T, Barnes H L, 2000. Reaction pathways in the Fe–S system below 100°C. Chemical Geology 167, 25–51.

Berner R A, 1967. Thermodynamic stability of sedimentary iron sulfides. American Journal of Science 265, 773–785.

Betelu S, Lerouge C, Berger G, Giffaut E, Ignatiadis I, 2012. Mechanistic study of pyrite reduction by hydrogen in NaCl 0.1 M at 90°C using electrochemical techniques. In 5th International meeting "Clays in natural and engineered barriers for radioactive waste confinement", Montpellier, France, 22–25 October 2012. Book of abstracts.

Biegler T, 1976. Oxygen reduction on sulphide minerals. Part II. Relation between activity and semiconducting properties of pyrite electrodes. J. Electroanal. Chem. 70, 265–275.

Biegler T, Swift D A, 1979. Anodic behaviour of pyrite in acid solutions. Electrochimica Acta 24, 415–420.

Bildstein O, Trotignon L, Perronnet M, Jullien M, 2006. Modelling iron–clay interactions in deep geological disposal conditions. Physics and Chemistry of the Earth 31, 618–625.

Borda M J, Strongin D R, Schoonen M A, 2003. A vibrational spectroscopic study of the oxidation of pyrite by ferric ion. Amer. Mineral. 88, 1318–1323.

Borda M J, Strongin D R, Schoonen M A, 2004. A vibrational spectroscopic study of the oxidation of pyrite by molecular oxygen. Geochimica et Cosmochimica Acta 68, 1807–1813.

Bosch J, Meckenstock R U, 2012. Rates and potential mechanism of anaerobic nitrate-dependent microbial pyrite oxidation. Biochemical Society Transactions 40, 1280–1283.

Bosch J, Lee K-Y, Jordan G, Kim K-W, Meckenstock R U, 2012. Anaerobic, nitrate-dependent oxidation of pyrite nanoparticles by *Thiobacillus denitrificans*. Environmental Science & Technology 46, 2095–2101.

Bruggeman C, Maes A, Vancluysen J, 2007. The identification of FeS_2 as a sorption sink for Tc(IV). Physics and Chemistry of the Earth 32, 573–580.

Brunner B, Yu J-Y, Mielke R E, MacAskill J A, Madzunkov S, McGenity T J, Coleman M, 2008. Different isotope and chemical patterns of pyrite oxidation related to lag and exponential growth phases of *Acidothiobacillus ferrooxidans* reveal a microbial growth strategy. Earth and Planetary Science Letters 270, 63–72.

Butler I B, Rickard D, 2000. Framboidal pyrite formation via the oxidation of iron (II) monosulfide by hydrogen sulphide. Geochimica et Cosmochimica Acta 64, 2665–2672.

Cabral T, Ignatiadis I, 2001. Mechanistic study of the pyrite–solution interface during the oxidative bacterial dissolution of pyrite (FeS_2) by using electrochemical techniques. International Journal of Mineral Processing 62, 41–64.

Cai Y, Pan Y, Xue J, Sun Q, Su G, Li X, 2009. Comparative XPS study between experimentally and naturally weathered pyrites. Applied Surface Science 255, 8750–8760.

Caldeira C L, Ciminelli V S T, Dias A, Osseo-Asare K, 2003. Pyrite oxidation in alkaline solutions: nature of the product layer. International Journal of Mineral Processing 72, 373–386.

Caldeira C L, Ciminelli V S T, Osseo-Asare K, 2010. The role of carbonate ions in pyrite oxidation in aqueous systems. Geochimica et Cosmochimica Acta 74, 1777–1789.

Chandra A P, Gerson A R, 2010. The mechanisms of pyrite oxidation and leaching: a fundamental perspective. Surface Science Reports 65, 293–315.

Chase M W (ed), 1985. JANAF thermochemical tables. 3rd ed. Part I, Al-Co; Part II, Cr-Zr. (Journal of Physical and Chemical Reference Data 14, Supplement 1)

Chase M W (ed), 1998. NIST-JANAF thermochemical tables. 4th ed. (Journal of Physical and Chemical Reference Data, Monograph 9)

Christidis G E, Huff W D, 2009. Geological aspects and genesis of bentonites. Elements 5, 93–98.

Ciminelli V S T, Osseo-Asare K, 1995. Kinetics of pyrite oxidation in sodium carbonate solutions. Metallurgical and Materials Transactions B 26, 209–218.

CRC, 1982. Handbook of chemistry and physics: a ready-reference book of chemical and physical data. 63rd ed. 1982–1983. Boca Raton, FL: CRC Press.

Cruz R, Bertrand V, Monroy M, González I, 2001. Effect of sulfide impurities on the reactivity of pyrite and pyritic concentrates: a multi-tool approach. Applied Geochemistry 16, 803–819.

Davison W, 1991. The solubility of iron sulphides in synthetic and natural waters at ambient temperature. Aquatic Sciences 53, 309–329.

de Donato P, Mustin C, Benoit R, Erre R, 1993. Spatial distribution of iron and sulphur species on the surface of pyrite. Applied Surface Science 68, 81–93.

Delécaut G, 2004. The geochemical behaviour of uranium in the Boom Clay. PhD thesis. Université catholique de Louvain, Belgium.

Descostes M, Mercier F, Beaucaire C, Zuddas P, Trocellier P, 2001. Nature and distribution of chemical species on oxidized pyrite surface: complementarity of XPS and nuclear microprobe analysis. Nuclear Instruments and Methods in Physics Research Section B 181, 603–609.

Descostes M, Beaucaire C, Mercier F, Savoye S, Sow J, Zuddas P, 2002. Effect of carbonate ions on pyrite (FeS_2) dissolution. Bulletin de la Societe Geologique de France 173, 265–270.

Descostes M, Vitorge P, Beaucaire C, 2004. Pyrite dissolution in acidic media. Geochimica et Cosmochimica Acta 68, 4559–4569.

Descostes M, Schlegel M L, Eglizaud N, Descamps F, Miserque F, Simoni E, 2010. Uptake of uranium and trace elements in pyrite (FeS_2) suspensions. Geochimica et Cosmochimica Acta 74, 1551–1562.

Druschel G, Borda M, 2006. Comment on "Pyrite dissolution in acidic media" by M. Descostes, P. Vitorge, and C. Beaucaire. Geochimica et Cosmochimica Acta 70, 5246–5250.

Elsetinow A R, Guevremont J M, Strongin D R, Schoonen M A A, Strongin M, 2000. Oxidation of {100} and {111} surfaces of pyrite: effects of preparation method. American Mineralogist 85, 623–626.

Fernández A M, Baeyens B, Bradbury M, Rivas P, 2004. Analysis of the porewater chemical composition of a Spanish compacted bentonite used in an engineered barrier. Physics and Chemistry of the Earth 29, 105–118.

Fukushi K, Sugiura T, Morishita T, Takahashi Y, Hasebe N, Ito H, 2010. Iron–bentonite interactions in the Kawasaki bentonite deposit, Zao area, Japan. Applied Geochemistry 25, 1120–1132.

Giannetti B F, Almeida C M V B, Bonilla S H, 2006. Electrochemical kinetic study of surface layer growth on natural pyrite in acid medium. Colloids and Surfaces A: Physicochemical and Engineering Aspects 272, 130–138.

Gleisner M, Herbert R B, Frogner Kockum P C, 2006. Pyrite oxidation by *Acidothiobacillus ferrooxidans* at various concentrations of dissolved oxygen. Chemical Geology 225, 16–29.

Grandia F, Domènech C, Arcos D, Duro L, 2006. Assessment of the oxygen consumption in the backfill. Geochemical modelling in a saturated backfill. SKB R-06-106, Svensk Kärnbränslehantering AB.

Grønvold F, Westrum E F, 1976. Heat capacities of iron disulfides from 5 to 700 K, pyrite from 300 to 780 K, and the transformation of marcasite to pyrite. The Journal of Chemical Thermodynamics 8, 1039–1048.

Guevremont J M, Elsetinow A R, Strongin D R, Bebie J, Schoonen M A A, 1998a. Structure sensitivity of pyrite oxidation: comparison of the (100) and (111) planes. American Mineralogist 83, 1353–1356.

Guevremont J M, Bebie J, Elsetinow A R, Strongin D R, Schoonen M A A, 1998b. Reactivity of the (100) plane of pyrite in oxidizing gaseous and aqueous environments: effects of surface imperfections. Environmental Science & Technology 32, 3743–3748.

Hamilton I C, Woods R, 1981. An investigation of surface oxidation of pyrite and pyrrhotite by linear potential sweep voltammetry. Journal of Electroanalytical Chemistry and Interfacial Electrochemistry 118, 327–343.

Heidel C, Tichomirowa, 2010. The role of dissolved molecular oxygen in abiotic pyrite oxidation under acid pH conditions – experiments with ^{18}O-enriched molecular oxygen. Applied Geochemistry 25, 1664–1675.

Hol A, van der Weijden R D, Van Weert G, Kondos P, Buisman C J N, 2010. Bio-reduction of pyrite investigated in a gas lift loop reactor. International Journal of Mineral Processing 94, 140–146.

Holmes P R, Crundwell F K, 2000. The kinetics of the oxidation of pyrite by ferric ions and dissolved oxygen: an electrochemical study. Geochimica et Cosmochimica Acta 64, 263–274.

Holmes P R, Fowler T A, Crundwell F K, 1999. The mechanism of bacterial action in the leaching of pyrite by *Thiobacillus ferrooxidans*. An electrochemical study. Journal of The Electrochemical Society 146, 2906–2912.

Huminicki D M C, Rimstidt J D, 2009. Iron oxyhydroxide coating of pyrite for acid mine drainage control. Applied Geochemistry 24, 1626–1634.

Hummel W, Berner U, Curti E, Pearson F J, Thoenen T, 2002. Nagra/PSI chemical thermodynamic data base 01/01. Parkland, FL: Universal Publishers, Section 5.6.3.

Jerz J K, Rimstidt J D, 2004. Pyrite oxidation in moist air. Geochimica et Cosmochimica Acta 68, 701–714.

Joeckel R M, Ang Clement B J, VanFleet Bates L R, 2005. Sulfate-mineral crusts from pyrite weathering and acid rock drainage in the Dakota Formation and Graneros Shale, Jefferson County, Nebraska. Chemical Geology 215, 433–452.

Jørgensen C J, Jacobsen O S, Elberling B, Aamand J, 2009. Microbial oxidation of pyrite coupled to nitrate reduction in anoxic groundwater sediment. Environmental Science & Technology 43, 4851–4857.

Kamyshny A, Goifman A, Gun, J, Rizkov D, Lev O, 2004. Equilibrium distribution of polysulfide ions in aqueous solutions at 25°C: a new approach for the study of polysulfides' equilibria. Environmental Science & Technology 38, 6633–6644.

Karnland O, 2010. Chemical and mineralogical characterization of the bentonite buffer for the acceptance control procedure in a KBS-3 repository. SKB TR-10-60, Svensk Kärnbränslehantering AB.

Karnland O, Olsson S, Nilsson U, 2006. Mineralogy and sealing properties of various bentonites and smectite-rich clay materials. SKB TR-06-30, Svensk Kärnbränslehantering AB.

Kaye G W C, Laby T H, 1986. Table of physical and chemical constants. 15th ed. London: Longman, Section 2.10.5.

Kaye & Laby, 2005. Tables of physical & chemical constants (16th edition 1995), Version 1.0. Available at http://www.kayelaby.npl.co.uk/ [25 October 2012].

Kelsall G H, Yin Q, Vaughan D J, England K E R, Brandon N P, 1999. Electrochemical oxidation of pyrite (FeS_2) in aqueous electrolytes. Journal of Electroanalytical Chemistry 471, 116–125.

King F, 2012. Gaseous hydrogen issues in nuclear waste disposal. In Gangloff R P, Somerday B P (eds). Gaseous hydrogen embrittlement of materials in energy technologies. Volume 1: the problem, its characterisation and effects on particular alloy classes. Cambridge: Woodhead Publishing, 126–148.

King F, Lilja C, Pedersen K, Pitkänen P, Vähänen M, 2010. An update of the state-of-the-art report on the corrosion of copper under expected conditions in a deep geologic repository. SKB TR-10-67, Svensk Kärnbränslehantering AB.

King F, Kolar M, Vähänen M, 2011a. Reactive-transport modelling of the sulphide-assisted corrosion of copper nuclear waste canisters. In Kursten B, Feron D, Druyts F (eds). Sulphur-assisted corrosion in nuclear disposal systems. Leeds, UK: Maney Publishing. (European Federation of Corrosion Publications 59), 152–164.

King F, Kolar M, Vähänen M, Lilja C, 2011b. Modelling long term corrosion behaviour of copper canisters in KBS-3 repository. Corrosion Engineering, Science and Technology 46, 217–222.

Kolaříková I, Švandová J, Přikryl R, Vinšová H, Jedináková-Křížová V, Zeman J, 2010. Mineralogical changes in bentonite barrier within Mock-Up-CZ experiment. Applied Clay Science 47, 10–15.

Laajalehto K, Leppinen J, Kartio I, Laiho T, 1999. XPS and FTIR study of the influence of electrode potential on activation of pyrite by copper or lead. Colloids and Surfaces A: Physicochemical and Engineering Aspects 154, 193–199.

Lambert J M, Simkovich G, Walker P L, 1980. Production of pyrrhotites by pyrite reduction. Fuel 59, 687–690.

Lambert J M, Simkovich G, Walker P L, 1998. The kinetics and mechanism of the pyrite-to-pyrrhotite transformation. Metallurgical and Materials Transactions B 29, 385–396.

Lange K, Rowe R K, Jamieson H, Flemming R L, Lanzirotti A, 2010. Characterization of geosynthetic clay liner bentonite using micro-analytical methods. Applied Geochemistry 25, 1056–1069.

Langmuir D, 1997. Aqueous environmental geochemistry. Upper Saddle River, NJ: Prentice Hall.

Lazo C, Karnland O, Tullborg E-L, Puigdomenech I, 2003. Redox properties of MX-80 and Montigel bentonite-water systems. In Finch R J, Bullen D B (eds). Scientific basis for nuclear waste management XXVI. Warrendale, PA: Materials Research Society. (Materials Research Society Symposium Proceedings 757), paper II8.1.

Lefticariu L, Pratt L A, LaVerne J A, Schimmelmann A, 2010. Anoxic pyrite oxidation by water radiolysis products – a potential source of biosustaining energy. Earth and Planetary Science Letters 292, 57–67.

Lehner S, Savage K, Ciobanu M, Cliffel D E, 2007. The effect of As, Co, and Ni impurities on pyrite oxidation kinetics: an electrochemical study of synthetic pyrite. Geochimica et Cosmochimica Acta 71, 2491–2509.

Licht S, Davis J, 1997. Disproportionation of aqueous sulphur and sulfide: kinetics of polysulfide decomposition. Journal of Physical Chemistry B 101, 2540–2545.

Liu R, Wolfe A L, Dzombak D A, Horwitz C P, Stewart B W, Capo R C, 2008. Electrochemical study of hydrothermal and sedimentary pyrite dissolution. Applied Geochemistry 23, 2724–2734.

Liu R, Wolfe A L, Dzombak D A, Horwitz C P, Stewart B W, Capo R C, 2009. Controlled electrochemical dissolution of hydrothermal and sedimentary pyrite. Applied Geochemistry 24, 836–842.

Lizama H M, Suzuki I, 1989. Rate equations and kinetic parameters of the reactions involved in pyrite oxidation by *Thiobacillus ferrooxidans*. Applied and Environmental Microbiology 55, 2918–2923.

Luther G W, 1987. Pyrite oxidation and reduction: molecular orbital theory consideration. Geochimica et Cosmochimica Acta 51, 3193–3199.

Macdonald D D, Sharifi-Asl S, 2011. Is copper immune to corrosion when in contact with water and aqueous solutions? Research Report 2011:09, Strålsäkerhetsmyndigheten (Swedish Radiation Safety Authority).

Marty N C M, Fritz B, Clément A, Michau N, 2010. Modelling the long term alteration of the engineered bentonite barrier in an underground radioactive waste repository. Applied Clay Science 47, 82–90.

Melamed A, Pitkänen O, 1994. Water-compacted Na-bentonite interaction in simulated nuclear fuel disposal conditions: the role of accessory minerals. In Barkatt A, Van Konynenburg R A (eds). Scientific basis for nuclear waste management XVII: symposium held in Boston, Massachusetts, USA, 29 November – 3 December. Pittsburgh, PA: Materials Research Society. (Materials Research Society Symposium Proceedings 333), 919–924.

Melamed A, Pitkänen O, 1996. Chemical and mineralogical aspects of water–bentonite interaction in nuclear fuel disposal conditions. VTT Research Notes 1766, Technical Research Centre of Finland.

Montes-H G, Fritz B, Clement A, Michau N, 2005a. Modeling of transport and reaction in an engineered barrier for radioactive waste confinement. Applied Clay Science 29, 155–171.

Montes-H G, Marty N, Fritz B, Clement A, Michau N, 2005b. Modelling of long-term diffusion-reaction in a bentonite barrier for radioactive waste confinement. Applied Clay Science 30, 181–198.

Montes-H G, Fritz B, Clement A, Michau N, 2005c. Modelling of geochemical reactions and experimental cation exchange in MX 80 bentonite. Journal of Environmental Management 77, 35–46.

Moses C O, Herman J S, 1991. Pyrite oxidation at circumneutral pH. Geochimica et Cosmochimica Acta 55, 471–482.

Moses C O, Nordstrom D K, Herman J S, Mills A L, 1987. Aqueous pyrite oxidation by dissolved oxygen and by ferric iron. Geochimica et Cosmochimica Acta 51, 1561–1571.

Moslemi H, Shamsi P, Habashi F, 2011. Pyrite and pyrrhotite open circuit potentials study: effects on flotation. Minerals Engineering 24, 1038–1045.

Murphy R, Strongin D R, 2009. Surface reactivity of pyrite and related sulfides. Surface Science Reports 64, 1–45.

Mycroft J R, Bancroft G M, McIntyre N S, Lorimer J W, Hill I R, 1990. Detection of sulphur and polysulphides on electrochemically oxidized pyrite surfaces by X-ray photoelectron spectroscopy and Raman spectroscopy. Journal of Electroanalytical Chemistry and Interfacial Electrochemistry 292, 139–152.

Nagra, 2002. Project Opalinus Clay. Safety report. Demonstration of disposal feasibility of spent fuel, vitrified high-level waste and long-lived intermediate-level waste (Entsorgungsnachweis). Nagra Technical Report NTB 02-05, Nagra, Switzerland.

Naveau A, Monteil-Rivera F, Guillon E, Dumonceau J, 2006. XPS and XAS studies of copper(II) sorbed onto a synthetic pyrite surface. Journal of Colloid and Interface Science 303, 25–31.

Nesbitt H W, Bancroft G M, Pratt A R, Scaini M J, 1998. Sulfur and iron surface states on fractured pyrite surfaces. American Mineralogist 83, 1067–1076.

Nicholson R V, Gillham R W, Reardon E J, 1988. Pyrite oxidation in carbonate-buffered solution: 1. Experimental kinetics. Geochimica et Cosmochimica Acta 52, 1077–1085.

Nicholson R V, Gillham R W, Reardon E J, 1990. Pyrite oxidation in carbonate-buffered solution: 21. Rate control by oxide coatings. Geochimica et Cosmochimica Acta 54, 395–402.

Ochs M, Lothenbach B, Shibata M, Yui M, 2004. Thermodynamic modelling and sensitivity analysis of porewater chemistry in compacted bentonite. Physics and Chemistry of the Earth 29, 129–136.

Ohkubo T, Kikuchi H, Yamaguchi M, 2008. An approach of NMR relaxometry for understanding water in saturated compacted bentonite. Physics and Chemistry of the Earth 33, S169–S176.

Ohmoto H, Hayashi K-I, Kajisa Y, 1994. Experimental study of the solubilities of pyrite in NaCl-bearing aqueous solutions at 250–350°C. Geochimica et Cosmochimica Acta 58, 2169–2185.

Puigdomenech I, Trotignon L, Kotelnikova S, Pedersen K, Griffault L, Michaud V, Lartigue J-E, Hama K, Yoshida H, West J M, Bateman K, Milodowski A, Banwart S A, Rivas Perez J, Tullborg E-L, 2000. O_2 consumption in a granitic environment. In Smith R W, Shoesmith D W (eds). Scientific basis for nuclear waste management XXIII: symposium held in Boston, Massachusetts, USA, 29 November – 2 December 1999. Warrendale, PA: Materials Research Society. (Materials Research Society Symposium Proceedings 608), 179–184.

Puigdomenech I, Ambrosi J-P, Eisenlohr L, Lartigue J-E, Banwart S A, Bateman K, Milodowski A E, West J M, Griffault L, Gustafsson E, Hama K, Yoshida H, Kotelnikova S, Pedersen K, Michaud V, Trotignon L, Rivas Perez J, Tullborg E-L, 2001. O_2 depletion in granitic media. The REX project. SKB TR-01-05, Svensk Kärnbränslehantering AB.

Pusch R, 2001. The buffer and backfill handbook. Part 2: materials and techniques. SKB TR-02-12, Svensk Kärnbränslehantering AB.

Pusch R, 2003. The buffer and backfill handbook. Part 3: models for calculation of processes and behaviour. SKB TR-03-07, Svensk Kärnbränslehantering AB.

Rand D A J, 1977. Oxygen reduction on sulphide minerals. Part III. Comparison of activities of various copper, iron, lead and nickel mineral electrodes. Journal of Electroanalytical Chemistry and Interfacial Electrochemistry 83, 19–32.

Rawlings D E, Tributsch H, Hansford G S, 1999. Reasons why *'Leptospirillum'*-like species rather than *Thiobacillus ferrooxidans* are the dominant iron-oxidizing bacteria in many commercial processes for the biooxidation of pyrite and related ores. Microbiology 145, 5–13.

Rickard D, 2006. The solubility of FeS. Geochimica et Cosmochimica Acta 70, 5779–5789.

Rickard D, Luther G W, 2007. Chemistry of iron sulfides. Chemical Reviews 107, 514–562.

Rimstidt J D, Vaughan D J, 2003. Pyrite oxidation: a state-of-the-art assessment of the reaction mechanism. Geochimica et Cosmochimica Acta 67, 873–880.

Robie R A, Hemingway B S, 1995. Thermodynamic properties of minerals and related substances at 298.15 K and 1 bar (10^5 pascals) pressure and at higher temperatures. U.S. Geological Survey Bulletin 2131.

Robie R A, Hemingway B S, Fisher J R, 1978. Thermodynamic properties of minerals and related substances at 298.15 K and 1 bar (10^5 pascals) pressure and at higher temperatures. U.S. Geological Survey Bulletin 1452.

Savage K S, Stefan D, Lehner S W, 2008. Impurities and heterogeneity in pyrite: influences on electrical properties and oxidation products. Applied Geochemistry 23, 103–120.

Schippers A, Jørgensen B B, 2001. Oxidation of pyrite and iron sulfide by manganese dioxide in marine sediments. Geochimica et Cosmochimica Acta 65, 915–922.

Schippers A, Jørgensen B B, 2002. Biogeochemistry of pyrite and iron sulfide oxidation in marine sediments. Geochimica et Cosmochimica Acta 66, 85–92.

Schoonen, M A A, 2004. Mechanisms of sedimentary pyrite formation. In Amend J P, Edwards K J, Lyons T W (eds). Sulfur biogeochemistry – past an present. Boulder, CO: Geological Society of America. (Geological Society of America Special Paper 379), 117–134.

Schoonen M, Elsetinow A, Borda M, Strongin D, 2000. Effect of temperature and illumination on pyrite oxidation between pH 2 and 6. Geochemical Transactions 4. doi:10.1039/b004044o.

Schoonen M A A, Harrington A D, Laffers R, Strongin D R, 2010. Role of hydrogen peroxide and hydroxyl radical in pyrite oxidation by molecular oxygen. Geochimica Cosmochimica et Acta 74, 4971–4987.

Scott T B, Riba Tort O, Allen G C, 2007. Aqueous uptake of uranium onto pyrite surfaces; reactivity of fresh versus weathered material. Geochimica Cosmochimica et Acta 71, 5044–5053.

Sidborn M, Neretnieks I, 2003. Modelling of biochemical processes in rocks: oxygen depletion by pyrite oxidation – model development and exploratory simulations. In Finch R J, Bullen D B (eds). Scientific basis for nuclear waste management XXVI. Warrendale, PA: Materials Research Society. (Materials Research Society Symposium Proceedings 757), paper II11.5.

Singh A K, Pourbaix A, 1997. E-pH diagrams for the Fe-S-H_2O system from 25 to 150°C. Cebelcor Report RT.318, Centre Belge d'Etude de la Corrosion.

SKB, 2010a. Corrosion calculations report for the safety assessment SR-Site. SKB TR-10-66, Svensk Kärnbränslehantering AB.

SKB, 2010b. Design, production and initial state of the buffer. SKB TR-10-15, Svensk Kärnbränslehantering AB.

SKB, 2011. Long-term safety for the final repository for spent nuclear fuel at Forsmark. Main report of the SR-Site project. Volume I. SKB TR-11-01, Svensk Kärnbränslehantering AB.

Szakálos P, Hultquist G, Wikmark G, 2007. Corrosion of copper by water. Electrochemical and Solid-State Letters 10, C63–C67.

Tao, D P, Li Y Q, Richardson P E, Yoon R-H, 1994. The incipient oxidation of pyrite. Colloids and Surfaces A: Physicochemical and Engineering Aspects 93, 229–239.

Tao D P, Richardson P E, Luttrell G H, Yoon R-H, 2003. Electrochemical studies of pyrite oxidation and reduction using freshly-fractured electrodes and rotating ring-disc electrodes. Electrochimica Acta 48, 3615–3623.

Taylor B E, Wheeler M C, Nordstrom D K, 1984. Stable isotope geochemistry of acid mine drainage: experimental oxidation of pyrite. Geochimica et Cosmochimica Acta 48, 2669–2678.

Techer I, Clauer N, Liewig N, 2009. Ageing effect on the mineral and chemical composition of Opalinus Clays (Mont Terri, Switzerland) after excavation and surface storage. Applied Geochemistry 24, 2000–2014.

Thomas J E, Skinner W M, Smart R St C, 2001. A mechanism to explain sudden changes in rates and products for pyrrhotite dissolution in acid solution. Geochimica et Cosmochimica Acta 65, 1–12.

Todd E C, Sherman D M, Purton J A, 2003. Surface oxidation of pyrite under ambient atmospheric and aqueous (pH=2 to 10) conditions: electronic structure and mineralogy from X-ray absorption spectroscopy. Geochimica et Cosmochimica Acta 67, 881–893.

Toniazzo V, Mustin C, Portal J M, Humbert B, Benoit, R, Erre R, 1999. Elemental sulfur at the pyrite surfaces: speciation and quantification. Applied Surface Science 143, 229–237.

Torrentó C, Cama J, Urmeneta J, Otero N, Soler A, 2010. Denitrification of groundwater with pyrite and *Thiobacillus denitrificans*. Chemical Geology 278, 80–91.

Toulmin P T, Barton P B, 1964. A thermodynamic study of pyrite and pyrrhotite. Geochimica et Cosmochimica Acta 28, 641–671.

Truche L, Berger G, Destrigneville C, Guillaume D, Giffaut E, 2010. Kinetics of pyrite to pyrrhotite reduction by hydrogen in calcite buffered solutions between 90 and 180°C: implications for nuclear waste disposal. Geochimica et Cosmochimica Acta 74, 2894–2914.

Usher C R, Cleveland C A, Strongin D R, Schoonen M A, 2004. Origin of oxygen in sulfate during pyrite oxidation with water and dissolved oxygen: an in situ horizontal attenuated total reflectance spectroscopy isotope study. Environmental Science & Technology 38, 5604–5606.

Van Loon L R, Glaus M A, Müller W, 2007. Anion exclusion effects in compacted bentonites: towards a better understanding of anion diffusion. Applied Geochemistry 22, 2536–2552.

Vaughan D J, 2005. Minerals/Sulphides. In Encyclopedia of geology. Amsterdam: Elsevier, 574–586.

von Oertzen G U, Skinner W M, Nesbitt H W, Pratt A R, Buckley A N, 2007. Cu adsorption on pyrite (100): *ab initio* and spectroscopic studies. Surface Science 601, 5794–5799.

Wagman D D, Evans W H, Parker V B, Schumm R H, Halow I, Bailey S M, Churney K L, Nuttall R L, 1982. The NBS tables of chemical thermodynamic properties: selected values for inorganic and C_1 and C_2 organic substances in SI units. New York: American Chemical Society. (Journal of Physical and Chemical Reference Data 11, Supplement 2)

Weerasooriya R, Tobschall H J, 2005. Pyrite–water interactions: effects of pH and pFe on surface charge. Colloids and Surfaces A: Physicochemical and Engineering Aspects 264, 68–74.

Weisener C, Gerson A, 2000. An investigation of the Cu(II) adsorption mechanism on pyrite by ARXPS and SIMS. Minerals Engineering 13, 1329–1340.

Wersin P, Spahiu K, Bruno J, 1994. Time evolution of dissolved oxygen and redox conditions in a HLW repository. SKB TR 94-02, Svensk Kärnbränslehantering AB.

Williamson M A, Rimstidt J D, 1994. The kinetics and electrochemical rate-determining step of aqueous pyrite oxidation. Geochimica et Cosmochimica Acta 58, 5443–5454.

Zhang G, Samper J, Montenegro L, 2008. Coupled thermo-hydro-bio-geochemical reactive transport model of CERBERUS heating and radiation experiment in Boom clay. Applied Geochemistry 23, 932–949.

Zhao W, Zhu H, Zong Z-M, Xia J-H, Wei X-Y, 2005. Electrochemical reduction of pyrite in aqueous NaCl solution. Fuel 84, 235–238.

Zhao W, Xu W-J, Zhong S-T, Zong Z-M, 2008. Desulfurization of coal by an electrochemical-reduction flotation technique. Journal of China University of Mining and Technology 18, 571–574.